



Application of modified *Sargassum duplicatum* biomass as an eco-friendly adsorbent for removing coomassie brilliant blue and phosphate ions from solution

B. Buhani¹ · A. B. Prayogo¹ · S. Suharso¹ · S. Sumadi² · S. Sutarto³

Received: 12 January 2024 / Revised: 9 May 2024 / Accepted: 14 May 2024

© The Author(s) under exclusive licence to Iranian Society of Environmentalists (IRSEN) and Science and Research Branch, Islamic Azad University 2024

Abstract

The modification of the surface of macro-alga *Sargassum duplicatum* (SD-Alg) using the cationic surfactant cetyl trimethyl ammonium chloride (CTACl) has been successfully carried out with the aim of creating a positively charged adsorbent surface (SD-Alg-CTA). The success of the SD-Alg modification is confirmed through FTIR for functional groups, SEM–EDX for composition, and XRD for crystallization. The ability of SD-Alg-CTA to adsorb anionic compounds such as coomassie brilliant blue (CBB) and phosphate ion (PIs) was tested through a series of experiments using the batch method. Adsorption data indicates that SD-Alg-CTA has the highest capacity to adsorb CBB dye at 87.54% at pH 5 and PIs at 96.75% at pH 4. The optimal contact time between CBB or PIs and SD-Alg-CTA is 120 min for CBB and 150 min for PIs. The interaction between CBB and PIs with SD-Alg-CTA tends to follow a pseudo second-order kinetic model and Freundlich adsorption isotherm model. The adsorption capacity of mono-component CBB and PIs by SD-Alg-CTA are 6.27×10^{-2} and 32.468×10^{-2} mmol g⁻¹, respectively, while the adsorption capacity of the bi-component mixture reaches 90.909 mmol g⁻¹. SD-Alg-CTA adsorbent can be used in 3 cycles of adsorption–desorption with the absorption rates of CBB and PIs remaining above 80%. SD-Alg-CTA stands out as a potential adsorbent for further development due to its high adsorption effectiveness, simple manufacturing procedure, and ability to be used repeatedly. This provides significant advantages in industrial applications that require the sustainable use of adsorbents.

Keywords *Sargassum duplicatum* · Adsorption · Coomassie brilliant blue dye · Phosphate compounds · Waste

Introduction

In today's modern era, environmental concerns are gaining increased attention due to population growth and intensified human activities. Among the most pressing environmental issues, water pollution stands out as it profoundly impacts water quality and aquatic ecosystems. The escalating usage of chemicals, particularly in industries such as textiles, fertilizers, and detergents, has become a major contributor to the current pollution crisis (Ahmad et al. 2019; Ibrahim et al. 2021). Dyes from various sources contain hazardous substances that persist in the environment, with some dyes breaking down into secondary pollutants that pose carcinogenic risks (Ozdemir et al. 2013).

Textile dyes like Coomassie Brilliant Blue R-250 (CBB) (Fig. 1a) often find their way into aquatic environments, where their lack of natural degradation under typical ecological conditions poses significant threats. Their presence not only alters the aesthetic appeal of water bodies but also

Editorial responsibility: Maryam Shabani.

✉ S. Suharso
suharso@fmipa.unila.ac.id

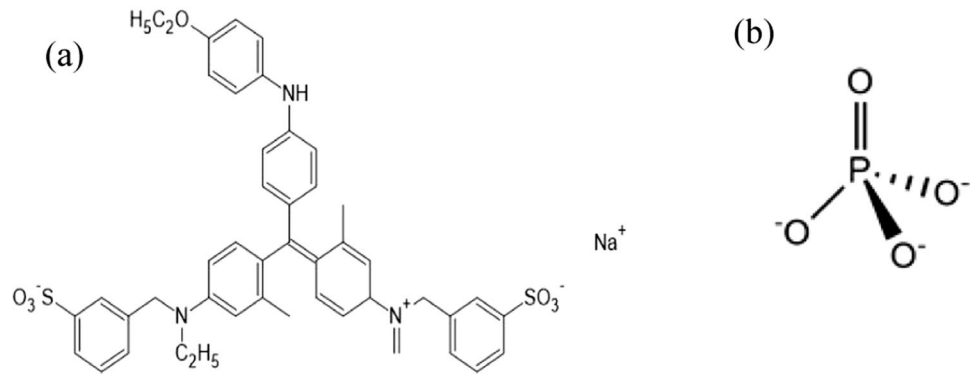
¹ Department of Chemistry, Faculty of Mathematic and Natural Sciences, University of Lampung, Jl. Soemantri Brojonegoro No. 1 Bandar Lampung, Lampung 35145, Indonesia

² Department of Electrical Engineering, Faculty of Engineering, University of Lampung, Jl. Soemantri Brojonegoro No. 1 Bandar Lampung, Lampung 35145, Indonesia

³ Department of Medicine, Faculty of Medicine, University of Lampung, Bandar Lampung 35141, Indonesia



Fig. 1 Chemical structures of **a** CBB and **b** PIs



leads to extensive harm in aquatic ecosystems by hindering light penetration and causing widespread poisoning (Altikatoğlu 2011; Abdel-Ghani et al. 2017).

In addition to colored dye substances, phosphate waste (PIs) (Fig. 1b) is another concerning chemical generated from fertilizer industries (Dolar et al. 2011) and excessive detergent use (Onyango et al. 2007). Soluble nutrient species from phosphate are significant pollutants, contributing to aquatic eutrophication, which fosters the proliferation of aquatic plants and algae while diminishing dissolved oxygen levels (Hamoudi et al. 2013; Yang et al. 2013). Considering the detrimental effects of unregulated discharge of textile dyes like CBB and PIs into the environment, particularly water bodies, proactive measures should be taken to treat wastewater containing these chemicals before releasing it into the environment.

Currently, adsorption methods are widely recognized and proven effective in addressing water pollution. Adsorption stands out as a preferred method due to its high efficiency, cost-effectiveness, and ease of operation. Nevertheless, conventional adsorbent materials often come with inherent limitations, such as low adsorption efficiency, high production costs, restricted pH interaction range, and limited applicability (Huang et al. 2017; Leo et al. 2011; Elwakeel et al. 2020; Elgarahy et al. 2021). Hence, there is an urgent imperative to develop efficient adsorbents capable of removing high-concentration chemical waste like CBB dyes and PIs from wastewater in an economically viable manner, while also being versatile across a broad pH spectrum (Nodeh et al. 2017; Buhani et al. 2023a).

Numerous endeavors have been undertaken to explore adsorbents derived from inexpensive, readily available materials that are naturally easy to produce and do not generate hazardous by-products for the environment. Such materials may include algal biomass (Buhani et al. 2021a) or biomass sourced from agricultural by-products (Yadav et al. 2015; Xu et al. 2010). The utilization of algal biomass as an adsorbent holds significant promise owing to its wide availability

and low production costs. Several studies have reported that algae, whether in living or biomass form, exhibit the capacity to adsorb chemical compounds (Flores-Chaparro et al. 2017; Lee et al. 2022).

However, the efficacy of algal biomass in binding chemical compounds is subject to certain limitations, such as its diminutive size, low density, and susceptibility to degradation by other microorganisms (Haris and Ramelow, 1990). Furthermore, the utility of algal biomass has been largely confined to adsorbing positively charged chemical compounds like metal ions and cationic dyes. This constraint stems from the presence of functional groups in algal biomass, including polysaccharides, proteins, amino, hydroxyl, carboxyl, sulfate ions, and others (Sayadi et al. 2018; Sarwa and Verma 2013).

Surface modification of the adsorbent has emerged as an intriguing strategy to enhance the adsorption properties of biomaterials for the efficient removal of both organic and inorganic pollutants (Adegoke et al. 2023; Buhani et al. 2019). Therefore, to broaden the applicability of algal biomass as an adsorbent for anionic chemical substances, modification is imperative using cationic agents to augment the number of active sites on the positively charged surface of algal biomass.

One effective method of surface modification of algal biomass involves the utilization of cationic surfactants, which can render the adsorbent rich in positive charges (Buhani et al. 2023b). Examples of such surfactants include cetyl trimethyl ammonium bromide (CTABr), hexadecyltrimethyl ammonium bromide (HDTMA-Br), and dodecyl benzyl dimethyl ammonium chloride (Jing et al. 2011; Yusof and Malek 2009; Bingol et al. 2009). Algal biomass adsorbents typically bear negative charges and possess active alkali or alkaline earth cation exchange groups. These active groups serve as charge balancers that can undergo exchange with other cations, such as cationic surfactants (Zhan et al. 2011).

To enhance the adsorption capacity of algal biomass as an adsorbent for anionic adsorbates such as CBB dyes and



PIs, this study has modified the biomass of the macro-alga *Sargassum duplicatum* (SD-Alg) using the cationic surfactant modifying agent cethyltrimethylammonium chloride (CTACl). SD-Alg biomass belongs to the brown algae group (*Phaeophyceae*) containing polysaccharides, polyphenols, and functional groups such as alcohol, carboxylate, ether, amine, amide, and fucoidan. These contents and functional groups make SD-Alg have significant potential for use as an adsorbent (Saldarriaga-Hernandez et al. 2020) and can be modified with CTACl surfactant to produce adsorption sites with positive charges through cation exchange reactions (Buhani et al. 2021b).

The modified adsorbent, SD-Alg-CTA, has been characterized using FTIR spectrometry and SEM–EDX to determine the functional group characteristics, morphology, and constituent elements of the adsorbent. Adsorption tests were conducted to analyze adsorption parameters, including kinetic and isotherm aspects, adsorption mechanisms, and the adsorbent's ability to be reused. SD-Alg-CTA adsorbent can be developed as an effective material for adsorbing chemical waste, whether cationic, neutral, or anionic, by leveraging the active groups from algal biomass and the cation exchange properties of CTACl. Therefore, the results of this study could be 1 solution to address the spread of dyes and other hazardous chemicals in the environment, especially in preventing increasing water pollution.

Materials and methods

Materials

In this study, the SD-Alg biomass used originates from Sebalang Sea, Lampung Province, Indonesia. The chemicals used are of analytical reagent (AR) grade from Merck, including cationic surfactant CTACl (25 wt%), CBB dye (98%), KH_2PO_4 (85%), KNO_3 (99.3%), KCl (99.9%), NaCl (99.8%), Na_2EDTA (99.9%), NaNO_3 (99%) M, HCl (37%), NaOH (99%), H_2SO_4 (97%), $(\text{NH}_4)_6\text{Mo}_7\text{O}_{24}$ (99%), SnCl_2 (98%), glycerol (85%), citrate, phosphate buffer, and methylene blue.

The chemical composition of SD-Alg biomass includes analysis of moisture content, ash, fat, protein, and carbohydrates determined based on proximate analysis and carbohydrates by the difference method. The characterization of adsorbent was conducted using SEM–EDX (Zeiss MA10, SEM–EDX, Gottingen, Germany) with the aim of understanding the surface morphology and identifying the constituent elements. The identification of adsorbent functional groups was performed through characterization using a Fourier-transform infrared spectrometer (Prestige-21 Shimadzu,

Japan). The crystallinity level of the adsorbent was analyzed using XRD (Rigaku Benchtop Miniplex 600, Japan).

The surface area of the adsorbent is determined using the methylene blue adsorption method (Abd El-Ghaffar et al. 2009). The following equation, Eq. 1, is used to calculate the surface area of the adsorbent.

$$A_s = \frac{10^{-20}}{M M_w} G N_{AV} \phi \quad (1)$$

whereas is the adsorbent surface area in $\text{m}^2 \text{g}^{-1}$, G the amount of methylene blue adsorbed (g) based on Langmuir adsorption capacity, N_{AV} the Avogadro's number (6.02×10^{23}), ϕ the methylene blue molecular cross-Sect. (197.2 \AA), M_w the molecular weight of methylene blue (373.9 g mol^{-1}) and M is the mass of adsorbent (g).

Furthermore, the surface charge was determined by analyzing the point of zero charge (pzc) of the adsorbent, determined using the solid addition method (Buhani et al. 2023b). A total of 0.1 g of adsorbent was mixed into a tube containing 20 mL of 0.1 M NaNO_3 . The initial pH was varied within the range of 3 to 12, adjusted using standard solutions of 0.1 M HCl for acidic conditions and 0.1 M NaOH for basic conditions. The solution was stirred using a shaker for 48 h. The supernatant was then measured for its pH. The pHpzc value was obtained from the plot of initial solution pH against supernatant pH.

Preparation of SD-Alg-CTA adsorbent

The modification procedure of SD-Alg-CTA is an adaptation of the method reported by (Guler et al. 2016; Buhani et al. 2021b). The modification process of SD-Alg involves the following steps: (1) SD-Alg biomass was initially washed with distilled water to remove impurities. (2) Subsequently, it was air-dried for 3 days and then oven-dried at $60 \text{ }^\circ\text{C}$ for 12 h. (3) The dried SD-Alg biomass is ground to a size of 100 mesh. (4) Then, 5 g of SD-Alg was mixed with a 1 M solution of NaCl (100 mL) in a reaction tube, stirred for 1 h, and left undisturbed for 24 h to enhance cation exchange capacity, resulting in SD-Alg-Na. (5) Separation of precipitate and filtrate is carried out. The obtained precipitate (SD-Alg-Na) was washed with distilled water until neutral pH is achieved, and then it was dried at room temperature. (6) Further, the creation of SD-Alg-CTA involved adding 2 g of SD-Alg-Na to a reaction tube containing 200 mL of CTACl solution with a concentration of 14 mmol L^{-1} . The mixture was stirred with a magnetic stirrer at a speed of 100 rpm and a temperature of $50 \text{ }^\circ\text{C}$ for 4 h. (7) The obtained precipitate was rinsed with distilled water until achieving a neutral pH and then dried at room temperature. It was subsequently



ground to a size of 100 mesh to produce the SD-Alg-CTA adsorbent.

Adsorption experiment

The adsorption study of CBB and PIs substances includes the determination of calibration curves, kinetic tests, adsorption equilibrium, and determination of the adsorption mechanism. To avoid possible interference, all adsorption tests were conducted under controlled conditions. The analyzed adsorption parameters include the influence of adsorption media, contact time, adsorbate concentration, as well as the adsorption mechanism and the repeated use of the adsorbent.

A 1000 mgL⁻¹ stock solution of CCB dye and KH₂PO₄ as a source of PIs was prepared and further used to obtain standard solutions by diluting the appropriate stock solution. All adsorption experiments were conducted at a temperature of 27 °C. The adsorption study of CBB and PIs was carried out using the batch method. Parameters investigated include the determination of the optimum pH of the medium, kinetics, and adsorption isotherms. The standard curve between absorbance (A) and the concentration of dye substances and PIs (C_o, mgL⁻¹) was measured using a UV–Vis spectrophotometer (Agilent Cary 100, U.S.A) at the maximum absorption wavelength of CBB dye (λ_{max} = 558 nm) and PIs (λ_{max} = 698 nm).

Mono-component adsorption for CBB or PIs solutions was performed by mixing the adsorbent and adsorbate at varying pH values between 3 and 12, contact times between 0 and 150 min, and adsorbate concentrations ranging from 0 to 300 mgL⁻¹. For bi-component adsorption (mixture of CBB or PIs dyes), it was conducted at the optimum pH and contact time obtained from the mono-component adsorption experiments with varying concentrations of the bi-component solution (0.01–0.35 mmol L⁻¹). The mono-component and bi-component adsorption processes were carried out in a shaker incubator at a temperature of 27 °C with a speed of 150 rpm. The mixture of filtrate and sediment was separated by centrifugation, and the filtrate was analyzed using a UV–Vis spectrophotometer. All adsorption experiments in this study were conducted with 3 repetitions. Specifically, for PIs, before analysis with a UV–Vis spectrophotometer, it was transformed into a phosphomolybdate ammonium complex by adding 20 mL of the PIs-containing solution to 20 mL of a molybdate reagent solution (2.5 g ammonium molybdate dissolved in 50 mL distilled water, then added 28 mL sulfuric acid). This solution was then added to a solution of SnCl₂ (12.5 g SnCl₂ in 50 mL glycerol) (Nodeh et al. 2017).

Adsorption studies were conducted to evaluate the influence of pH, contact time, and concentration on the removal of CBB and PIs by the adsorbent. The removal efficiency (%)

and adsorption capacity at equilibrium conditions (q_e) and at a specific time (q_t) were calculated based on the Eqs. 2–4:

$$\text{Adsorption}(\%) = \frac{(C_o - C_t)}{C_o} \times 100 \quad (2)$$

$$q_e = \frac{(C_o - C_e)}{m} \times V \quad (3)$$

$$q_t = \frac{(C_o - C_t)}{m} \times V \quad (4)$$

where C_o , C_e , and C_t respectively represent the initial concentration, equilibrium concentration, and concentration at time (t) (mg L⁻¹), V represents the volume of the solution (L) containing CBB or PIs, and m describes the mass of the adsorbent (g).

Sequential desorption

To determine the dominant interactions occurring between CBB and PIs with the adsorbent, the first step involves the adsorption process of both adsorbates under all optimal adsorption conditions (pH, contact time, and optimum concentration). Subsequently, the adsorption interactions were determined through the method of sequential desorption. The trapping mechanisms were identified through desorption using deionized water as the eluent, ion exchange with a 0.1 M KNO₃, electrostatic interactions with 0.1 M HCl, and complex formation with a 0.1 M Na₂EDTA solution.

Reuse of adsorbent

The ability of the adsorbent to be reused was investigated by conducting adsorption experiments under optimal conditions. CBB or PIs that have been adsorbed by SD-Alg-CTA were released using an eluent consisting of a 50 mL solution of 0.1 M HCl. The adsorption–desorption process was repeated several times until the adsorption percentage of CBB or PIs is less than 60%.

Results and discussion

Characteristics of adsorbents SD-Alg, SD-Alg-Na, and SD-Alg-CTA

Surface modification of SD-Alg begins by interacting SD-Alg with Na⁺ ion exchange agents, resulting in SD-Alg-Na aimed at enhancing cation exchange capacity. The next step

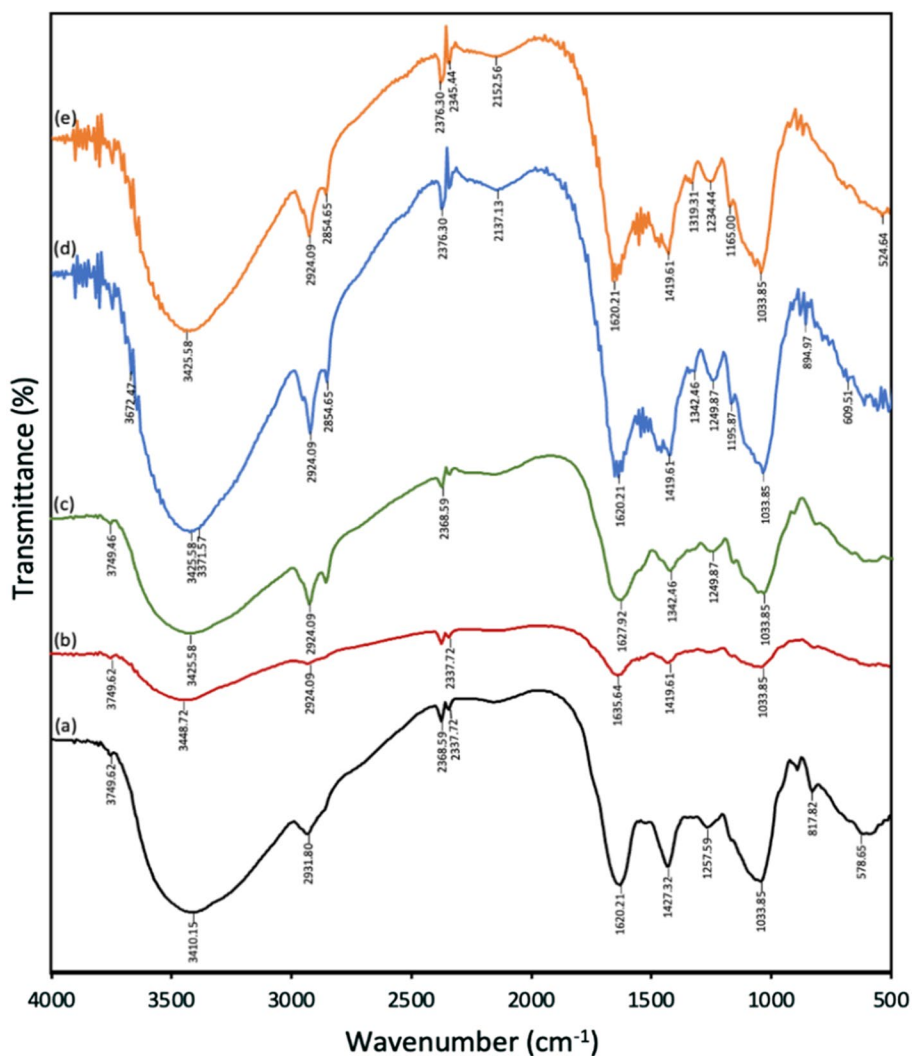


involves cation exchange reactions with CTACl to produce SD-Alg-CTA. The SD-Alg biomass used in this study exhibited proximate content as follows: ash (2.18%), moisture (30.2%), carbohydrates (64.57%), protein (2.24%), and fat (0.81%). Characterization of these 3 adsorbents was carried out by identification of adsorbent functional groups was performed using FTIR spectrometry and analyzing the surface morphology and quantification of the main constituent elements present in the adsorbent using SEM–EDX. Analysis using XRD is conducted to determine the level of crystallinity of the adsorbent, as well as the analysis of the surface area and charge of the adsorbent.

The success of cation exchange on SD-Alg with CTAC can be identified through changes in the FTIR spectra in SD-Alg-Na and SD-Alg-CTA. In SD-Alg (Fig. 2a), a broad FTIR peak is observed between 3700 and 3400 cm^{-1} associated with the OH bond of hydroxyl groups, and at a wavenumber of 3410.15 cm^{-1} , there is a primary N–H group overlapping with the –OH group in SD-Alg (Kim

et al. 2020). Then, there is an absorption at a wavenumber of 2931.80 cm^{-1} , indicating the presence of C–H groups from a carbon chain (aliphatic) CH_2 (Buhani et al. 2023a). The characteristic C=O group of carboxylic acid in SD-Alg is indicated by the absorption band at a wavenumber of 1620.21 cm^{-1} . In Fig. 2b, which represents the spectrum of SD-Alg-Na, there is absorption at the same wavenumbers as SD-Alg and additional absorption at a wavenumber of 1419.61 cm^{-1} , indicating the presence of O–Na groups (Na cation bonding with O in the carboxylate group), indicating the formation of SD-Alg-Na (Guler et al. 2016; Buhani et al. 2021b). Furthermore, in SD-Alg-CTA (Fig. 2c), all the characteristic FTIR spectrum features of SD-Alg appear, with an additional new absorption at a wavelength of 1342.46 cm^{-1} , indicating the presence of C–H groups from the – CH_3 group of CTACl (Guler et al. 2016; Buhani et al. 2023a).

Fig. 2 FTIR Spectra of **a** SD-Alg, **b** SD-Alg-Na, **c** SD-Alg-CTA, **d** SD-Alg-CTA with CBB, and **e** SD-Alg-CTA with PIs



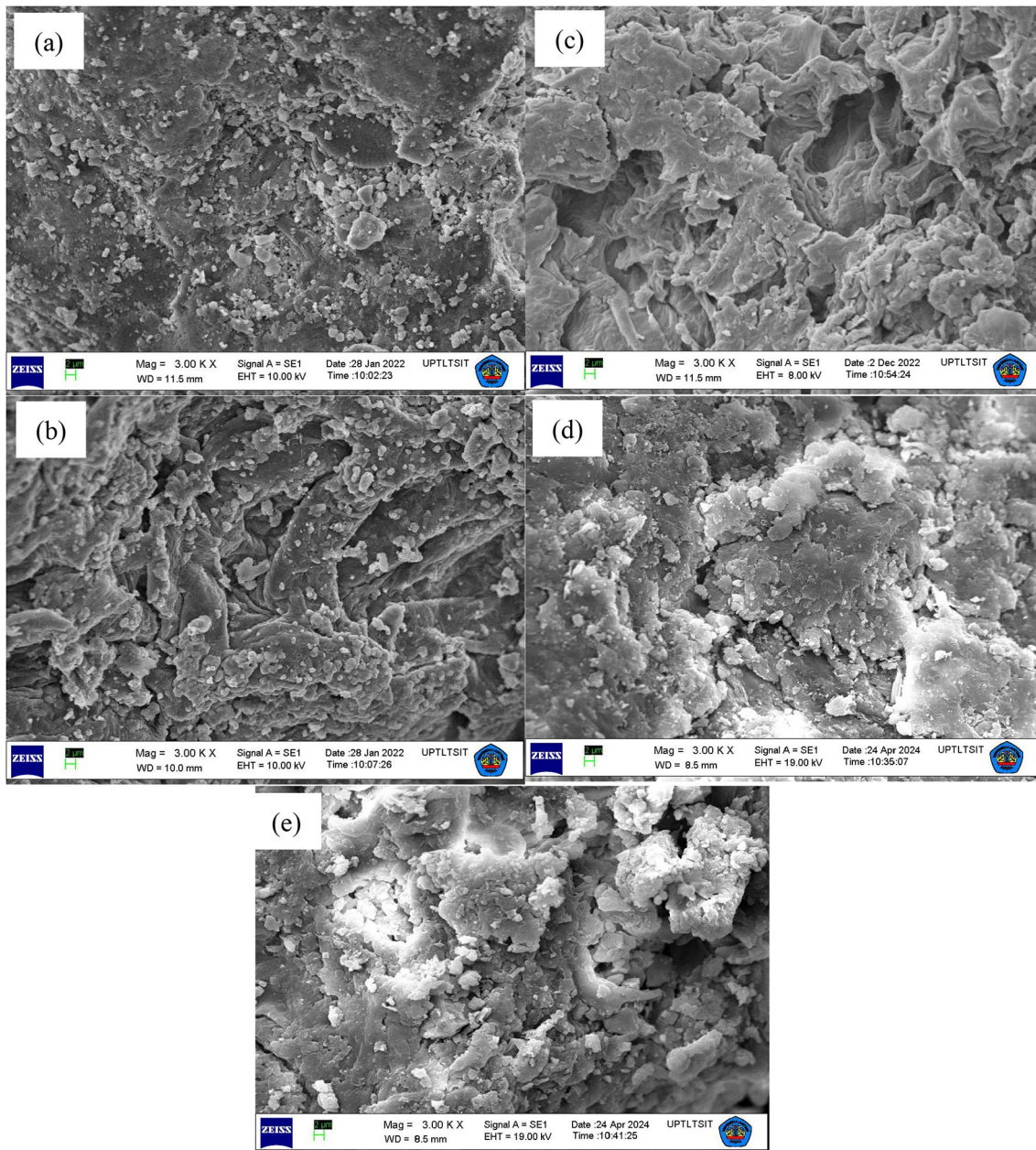


Fig. 3 SEM of **a** SD-Alg, **b** SD-Alg-Na, **c** SD-Alg-CTA, **d** SD-Alg-CTA with CBB, and **e** SD-Alg-CTA with PIs

The adsorption results of SD-Alg-CTA on CCB (Fig. 2d) and PIs (Fig. 2e) exhibit spectra patterns relatively similar to SD-Alg-CTA (Fig. 2c). The presence of CBB adsorbed onto SD-Alg-CTA (Fig. 2d) is indicated by absorption in the region around $1200\text{--}800\text{ cm}^{-1}$ originating from O-S vibration (Escalona Platero et al. 1996). Furthermore, the IR spectrum of the adsorption results of SD-Alg-CTA with PiS (Fig. 2e) shows strong absorption around $1200\text{--}900\text{ cm}^{-1}$, indicating the presence of O-P vibration from phosphate ions (Jastrzębski et al. 2011). The presence of adsorbed CBB and

PIs by SD-Alg-CTA is further identified through elemental constituent analysis using EDX.

Surface morphology analysis of the 3 adsorbents was conducted by observing the SEM (Fig. 3) results coupled with semi-quantitative analysis of the major constituent elements using EDX (Fig. 4 and Table 1). From the SEM analysis results, it can be observed that in SD-Alg (Fig. 3a), the surface morphology is quite homogeneous but not contrasting, while in SD-Alg-Na (Fig. 3b), the

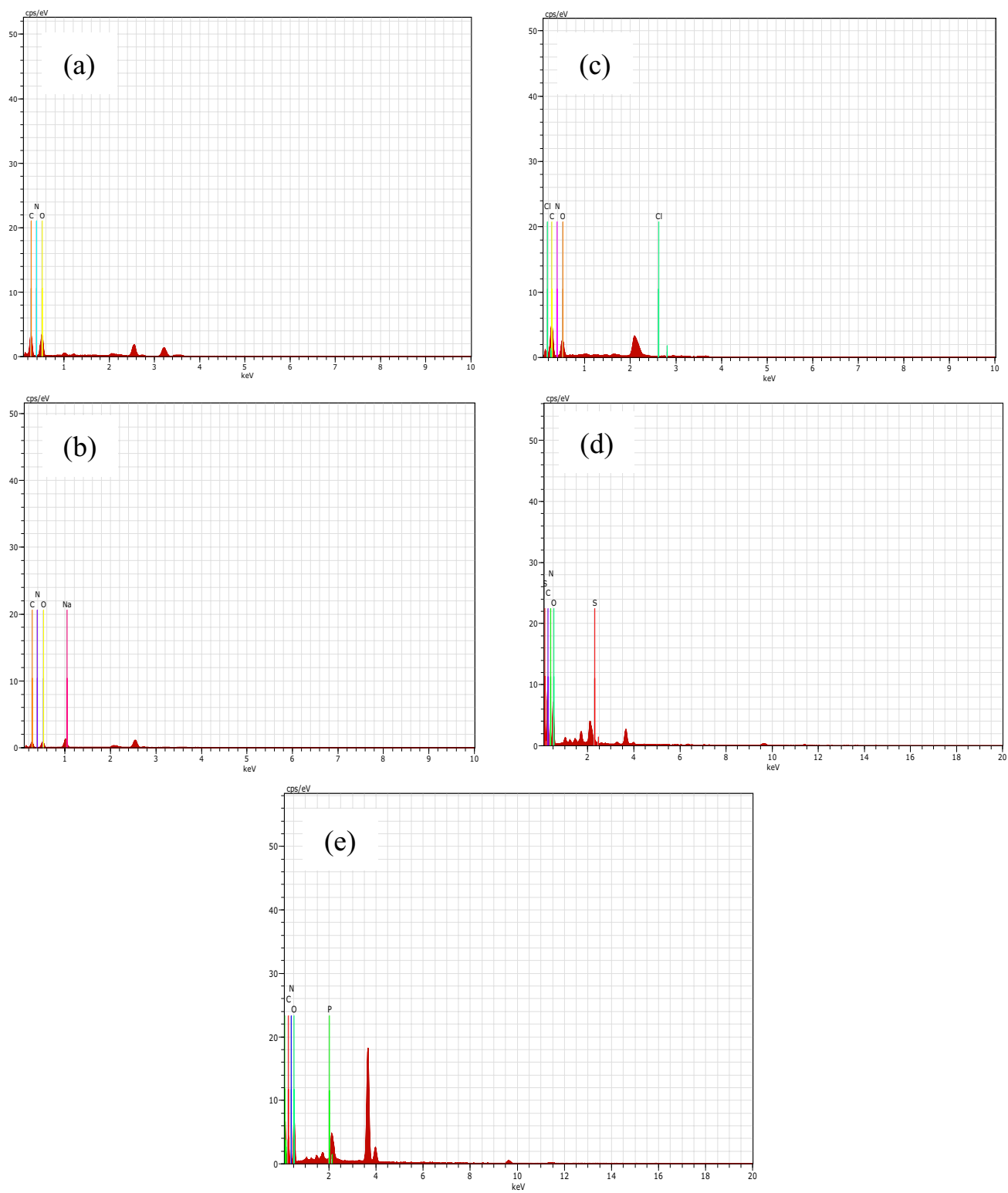
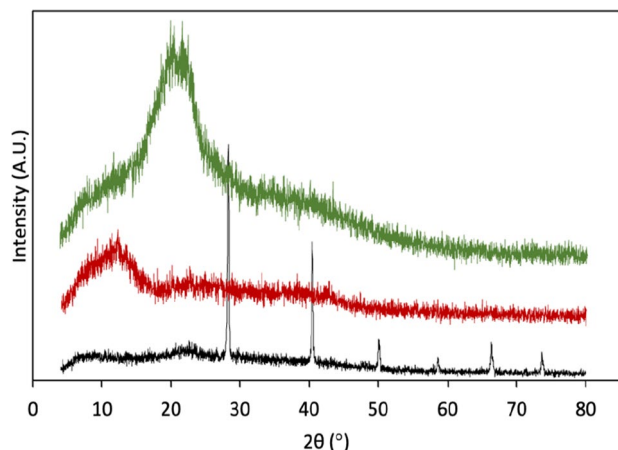


Fig. 4 EDX spectra of **a** SD-Alg, **b** SD-Alg-Na, **c** SD-Alg-CTA, **d** SD-Alg-CTA with CBB, and **e** SD-Alg-CTA with PIs

Table 1 Data on the constituent elements in the adsorbent before and after adsorption of CBB and PIs from SD-Alg, SD-Alg-Na, and SD-Alg-CTA

Materials	Element/Weight, (%)						Element/Atomic, (%)					
	O	C	N	Na	S	P	O	C	N	Na	S	P
SD-Alg	54.42	41.05	4.53	–	–	–	47.62	47.85	4.53	–	–	–
SD-Alg-Na	36.94	37.55	1.15	24.36	–	–	35.11	47.53	1.25	16.11	–	–
SD-Alg-CTA	42.28	51.42	6.30	–	–	–	35.84	58.06	6.10	–	–	–
SD-Alg-CTA-CBB	50.85	42.90	5.21	–	1.04	–	44.43	49.91	5.20	–	0.46	–
SD-Alg-CTA-PIs	61.08	32.41	4.27	–	–	2.24	55.38	39.14	4.43	–	–	1.05

**Fig. 5** XRD patterns of a SD-Alg, b SD-Alg-Na, and c SD-Alg-CTA

surface is non-homogeneous but more contrasting compared to the morphology of SD-Alg. In SD-Alg-CTA (Fig. 3c), it can be seen that the surface morphology tends to be more homogeneous and contrasting compared to SD-Alg and SD-Alg-Na. This indicates that a change in the surface morphology has occurred in SD-Alg-CTA due to the cation exchange interaction with CTACl. This is further supported by the EDX analysis results (Fig. 4 and Table 1), which show semi-quantitative data of the major constituent elements in the adsorbents before and after adsorption. In Fig. 4 and Table 1, it can be observed that there is an increase in the % of C and N elements in SD-Alg-CTA (Fig. 4c) compared to SD-Alg (Fig. 4a). The percentage of C and N elements in SD-Alg is 47.86 and 4.53%, respectively, and in SD-Alg-CTA, they become 58.06 and 6.10%, respectively. The increase in the % of C and N elements in SD-Alg-CTA is derived from the CTACl surfactant, indicating that the cation exchange reaction with Na^+ ions has occurred, resulting in the formation of SD-Alg-CTA.

The surface morphology of SD-Alg-CTA after adsorbing CBB (Fig. 3d) and PIs (Fig. 3e) shows more pronounced changes compared to SD-Alg-CTA before adsorption (Fig. 3c). This is also supported by the EDX data,

which indicates an increase in the composition of elements within SD-Alg-CTA originating from the adsorbates CBB (Fig. 4d) and PIs (Fig. 4e). In the SD-Alg-CTA-CBB material (Fig. 4d and Table 1), there is an additional presence of S elements originating from CBB, while in the SD-Alg-CTA-PIs material (Fig. 4e and Table 1), there is an additional presence of P elements from PIs. The EDX analysis data aligns with the results of the IR analysis (Fig. 2d and 2e).

In Fig. 5, the differences in XRD diffraction patterns of SD-Alg, SD-Alg-Na, and SD-Alg-CTA are shown. From Fig. 5a, it can be observed that the XRD spectrum of SD-Alg exhibits several sharp peaks indicating its crystalline nature, with dominant mineral content derived from CaCO_3 and KCl (Milledge et al. 2020). The XRD spectrum of SD-Alg-Na (Fig. 5b) and SD-Alg-CTA (Fig. 5c) both show an amorphous shape. This indicates ion exchange by Na^+ ions in SD-Alg-Na and exchange with CTA^+ ions in SD-Alg-CTA has altered its structure to an amorphous form (Guler et al. 2016).

The surface area characteristics of the adsorbents obtained using the methylene blue adsorption method (Abd El-Ghaffar et al. 2009) on SD-Alg, SD-Alg-Na, and SD-Alg-CTA were found to be 147.58, 162.44, and 171.897 $\text{m}^2 \text{g}^{-1}$, respectively. From this data, it can be inferred that ion exchange on SD-Alg with Na^+ ions result in SD-Alg-Na, and ion exchange of Na^+ ions on SD-Alg-Na with CTA^+ ions results in SD-Alg-CTAC, thereby increasing the surface area of the material. Furthermore, the analysis results of the pH_{PZC} values of SD-Alg, SD-Alg-Na, and SD-Alg-CTA are as follows: 8.02, 8.00, and 7.03, respectively. Determination of the pH_{PZC} value aims to understand the influence of pH on the surface charge of the adsorbent. The surface charge of the adsorbent will be negative at $\text{pH} > \text{pH}_{\text{PZC}}$ and positive at $\text{pH} < \text{pH}_{\text{PZC}}$ (Ai et al. 2011).

Effect of pH on the % adsorption of CBB and PIs

Figure 6 illustrates the influence of solution pH on the adsorption of CBB and PIs by the adsorbents SD-Alg, SD-Alg-Na, and SD-Alg-CTA. As depicted in Fig. 6, it can be

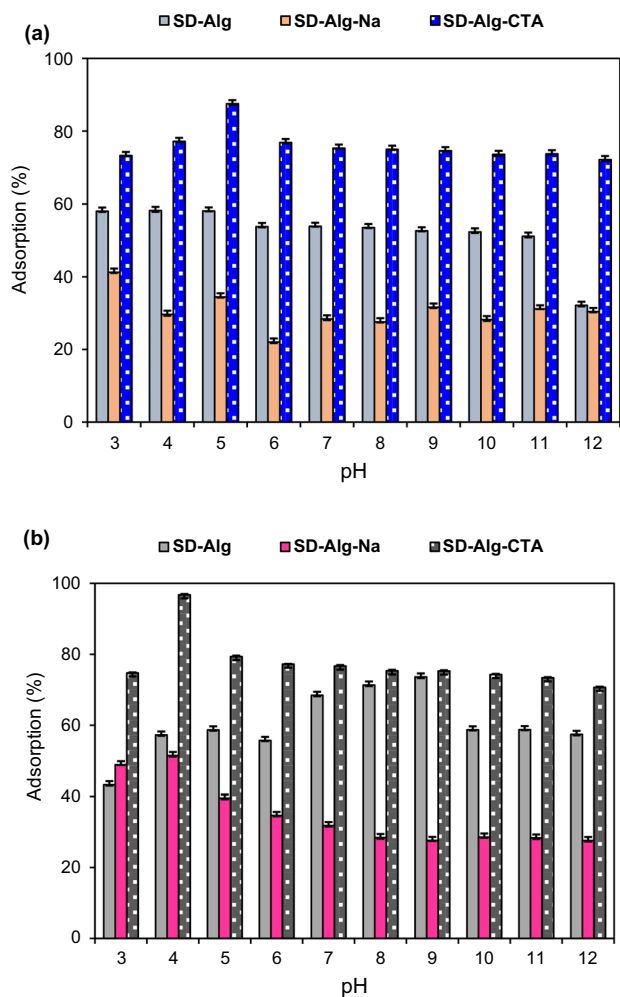


Fig. 6 Effect of solution pH parameters on the adsorption percentage of **a** CBB and **b** PIs (adsorbent mass: 0.1 g; solution volume: 25 mL; C_0 : 10 mg L^{-1} ; temperature: $27 \pm 1 \text{ }^\circ\text{C}$; agitation speed: 150 rpm; time: 60 min)

observed that the % adsorption of CBB and PIs follows the sequence $\text{SD-Alg} < \text{SD-Alg-Na} < \text{SD-Alg-CTA}$. This indicates that the modification of SD-Alg with the surfactant CATCl has successfully increased the % adsorption of anionic substances such as CBB and phosphate ions. These results align with the research reported by Buhani et al. 2023b, stating that anionic dyes like methyl orange are more adsorbed by adsorbents with a positive surface resulting from electrostatic interactions between positive and negative charges.

The data in Fig. 6a and b indicate that CBB and PIs are adsorbed most significantly by SD-Alg-CTA at pH 5 (87.54%) and pH 4 (96.75%), respectively. Increasing the pH value does not significantly reduce the percentage of CBB adsorbed on SD-Alg-CTA. In general, it can be observed

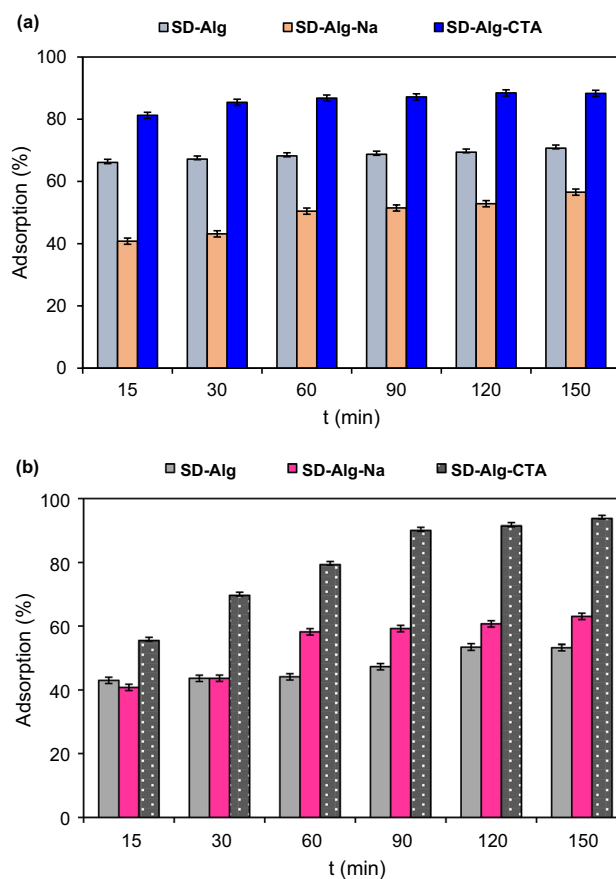


Fig. 7 Influence of contact time on % adsorption of **a** CBB and **b** PIs by SD-Alg, SD-Alg-Na, and SD-Alg-CTA (adsorbent mass: 0.1 g; solution volume: 10 mL; C_0 : 10 mg L^{-1} ; temperature: $27 \pm 1 \text{ }^\circ\text{C}$; agitation speed: 150 rpm; CBB dye (pH 5) and PIs (pH 4))

that the interaction between CBB and PIs with SD-Alg-CTA occurs at low pH. This is supported by the pH_{pzc} analysis data of SD-Alg-CTA, which has a value of 7.03, indicating that the adsorbent surface is positively charged under these conditions. Thus, the optimum interaction between CBB and PIs is more likely to occur at $\text{pH} < \text{pH}_{\text{pzc}}$ and begins to decline at $\text{pH} > \text{pH}_{\text{pzc}}$. The interaction between CBB and PIs occurs through electrostatic interactions between the positively charged SD-Alg-CTA and the negatively charged CBB or PIs (Li et al. 2008; Huang et al. 2015; Hussain et al. 2021). At low pH, it is assumed that protonation of the electrostatic interactions between the adsorbate and adsorbent will drive high adsorption efficiency (Nodeh et al. 2017). The decrease in adsorption at high pH is caused by the competitive adsorption of hydroxide ions (OH^-) between CBB or PIs to the active sites of the adsorbent (Buhani et al. 2019; Nodeh et al. 2017).



Influence of contact time

The influence of contact time between the adsorbed CBB and PIs is presented in Fig. 7. From the data in Fig. 7a and b, it can be observed that CBB and PIs exhibit a higher percentage of adsorption on SD-Alg-CTA compared to SD-Alg and SD-Al-CTAC. This is consistent with the findings from the investigation on the influence of pH discussed earlier.

The data in Fig. 7a indicates that with an increase in contact time, there is an increase in the percentage of CBB dye adsorbed on all 3 adsorbents, although not as significant as the increase in the percentage of PIs (Fig. 7b). In Fig. 7a, it can be observed that the contact time between CBB and SD-Alg-CTA in the first 15 min resulted in 81.25% CBB adsorbed, reaching an optimum at a contact time of 120 min with 88.46% adsorption. There is a

decrease in adsorption at a contact time of 150 min. Furthermore, the influence of contact time on the percentage of adsorbed PIs is observed in Fig. 7b, where the first 15 min of contact time resulted in 55.44%, and at a contact time of 150 min, 93.73% PIs were adsorbed. The optimum contact time data for the interaction between CBB and PIs is then used as the optimum contact time in the subsequent experiments.

Kinetics of adsorption

The kinetics of CBB and PIs adsorption by SD-Alg, SD-Alg-Na, and SD-Alg-CTA were studied by analyzing the data obtained from the variation in adsorption contact time against the % adsorbed CBB and PIs, as shown in Fig. 7. The experimental data presented in Fig. 7 were analyzed using the pseudo-first-order, pseudo-second-order, intra-particle

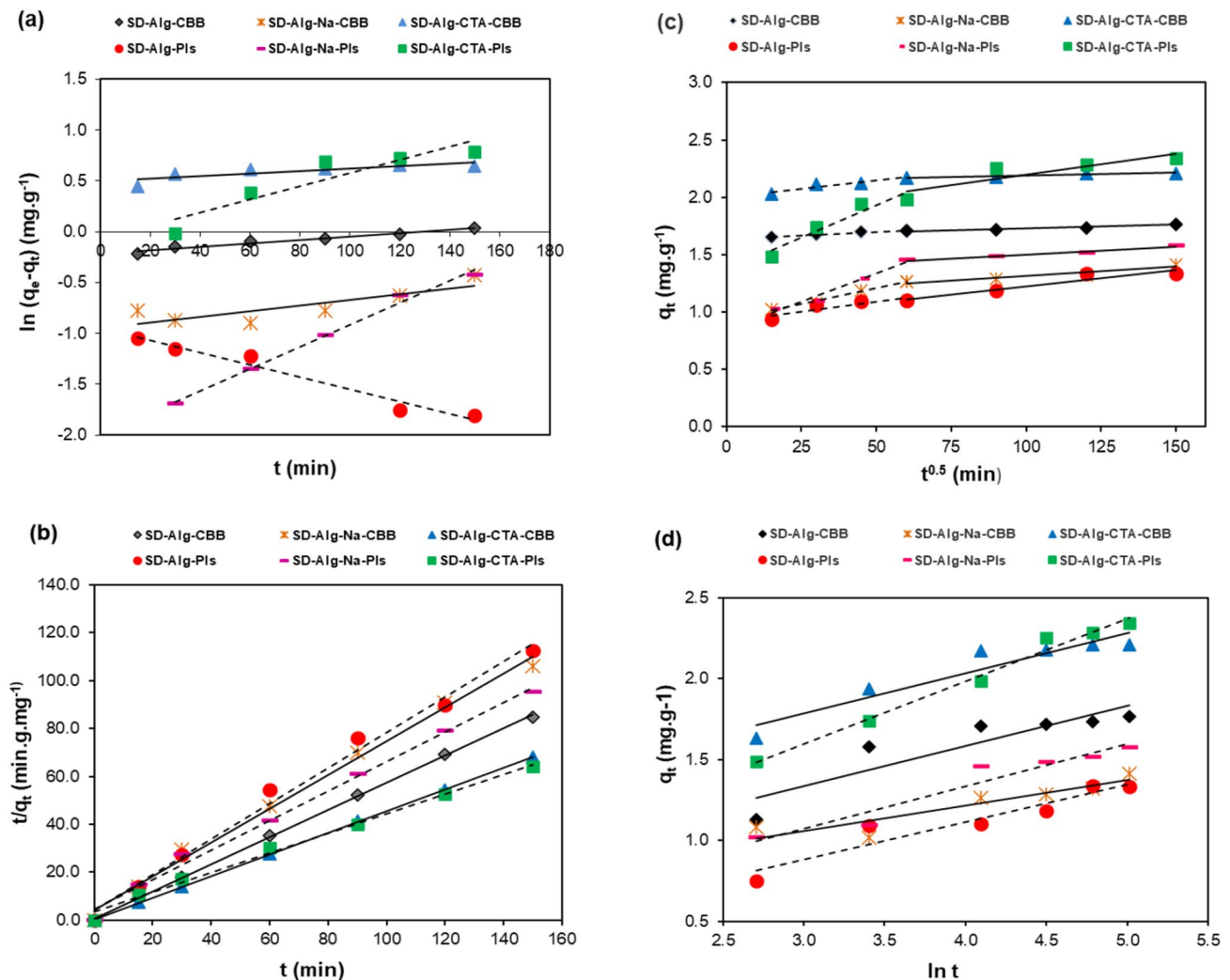


Fig. 8 Regression analysis of the adsorption CBB and PIs on SD-Alg, SD-Alg-Na, and SD-Alg-CTA by **a** Pseudo-first-order equation, **b** Pseudo second order equation, **c** Intra particle diffusion model, and **d** Elovich equation



Table 2 Kinetics parameters of CBB and PIs adsorption by SD-Alg, SD-Alg-Na, and SD-Alg-CTA (adsorbent mass: 0.1 g; solution volume: 10 mL; C_0 : 10 mg L⁻¹; temperature: 27 ± 1 °C; agitation speed: 150 rpm; CBB dye (pH 5) and PIs (pH 4))

Adsorbate		CBB			PIs		
Adsorbent		SD-Alg	SD-Alg-Na	SD-Alg-CTA	SD-Alg	SD-Alg-Na	SD-Alg-CTA
Kinetic models	Parameters						
Pseudo first order	q_e (exp) (mg g ⁻¹)	1.768	1.414	2.207	1.332	1.576	2.343
	$k_1 \times 10^{-3}$ (min ⁻¹)	1.700	2.800	1.200	6.000	10.900	6.500
	R^2	0.961	0.696	0.699	0.967	0.992	0.840
Pseudo second order	$k_2 \times 10^{-3}$ (g mg ⁻¹ min ⁻¹)	0.483	0.117	0.474	0.128		
	0.083	0.049					
	R^2	0.997	0.994	0.999	0.991	0.994	0.993
Intra particle diffusion	Initial linear portion						
	k_{ip1} (mg g ⁻¹ min ^{-0.5})	0.014	0.064	0.034	0.043	0.114	0.134
	C_1 (mg g ⁻¹)	1.600	0.756	1.911	0.791	0.536	0.992
	R_1^2	0.977	0.968	0.936	0.871	0.933	0.964
	Second linear portion						
	k_{ip2} (mg g ⁻¹ min ^{-0.5})	0.013	0.032	0.010	0.057	0.026	0.076
	C_2 (mg g ⁻¹)	1.597	0.977	2.093	0.667	1.240	1.444
	R_2^2	0.926	0.865	0.842	0.907	0.939	0.857
	Elovich	α (mg g ⁻¹ min ⁻¹)	2.719	6.766	16.025	0.513	0.802
β (g mg ⁻¹)		4.034	6.378	4.011	4.305	3.840	2.578
R^2		0.813	0.842	0.894	0.743	0.935	0.986

diffusion models, and Elovich each employing Eqs. 5–8, with the results of the analysis presented in Fig. 8 and Table 2.

$$\log(q_e - q_t) = \log q_e - \frac{k_1}{2.303} t \quad (5)$$

$$\frac{t}{q_t} = \frac{1}{k_2 q_e^2} + \frac{t}{q_e} \quad (6)$$

$$q_t = k_{id} t^{0.5} + C \quad (7)$$

$$qt = \frac{1}{\beta} \ln(\alpha\beta) + \frac{1}{\beta} \ln t \quad (8)$$

where q_t and q_e (mg g⁻¹) are total CBB dye or PIs adsorption capacity at time (t) and at equilibrium, respectively, k_1 and k_2 are the first order and second order rate constants, respectively. In addition, k_{id} (mg g⁻¹ min^{-0.5}) is the intra-particle diffusion rate constant, and C value (mg g⁻¹) represents a constant depicting resistance to mass transfer in the boundary layer. In the Elovich kinetic model, the initial rate and

adsorption capacity are described by the parameters α (mg g⁻¹ min⁻¹) and β (g mg⁻¹), respectively.

Based on Table 2, it can be observed that the pseudo-second-order kinetic model has the best correlation coefficient (R^2) compared to the pseudo-first-order and Elovich model, both for CBB and PIs on all 3 adsorbents. The pseudo-second-order kinetic model assumes that the adsorption capacity is proportional to the number of active sites on the adsorbent. Thus, this kinetic model suggests that chemisorption is the rate-limiting step of adsorption at fixed locations without interaction between adsorbates. However, similar to the pseudo-first-order model, rapid and controlled diffusion exchange is usually considered in the adsorption of solutes from a solvent (Boparai et al. 2011). The Elovich kinetic model is more suitable for describing adsorption processes that occur chemically and is suitable for systems with highly heterogeneous surfaces (Aharoni et al. 1970). When the surface coverage is low, the influence of interactions between adsorbed species does not significantly affect the kinetics (Ferreira et al. 2019; Al-Odayni et al. 2023). In this study, interactions between the adsorbent and adsorbate may occur through



multiple mechanisms. Therefore, the Elovich kinetic model is less appropriate for explaining the interactions of the 3 adsorbents (SD-Alg, SD-Alg-Na, and SD-Alg-CTA) with CBB and PIs. In general, the pseudo-second-order model is more dominant, indicating that chemisorption occurs in several stages of adsorption between the adsorbate and adsorbent through electrostatic interactions (Aqdam et al. 2021).

Furthermore, to investigate the adsorbate diffusion process by the adsorbent in simulating kinetic data (Dogan et al. 2009), the data in Fig. 7 were also analyzed with the intra-particle diffusion (IPD) model. The results of this analysis are presented in Fig. 8c and Table 2. From Fig. 8c, it can be observed that all plots have 2 linear segments. The first part represents the initial period with a contact time of 0–60 min, depicting external mass transfer. The second part is the adsorption period (60–150 min), representing a pattern that describes intra-particle diffusion. The second linear part does not pass through the origin ($C \neq 0$), indicating that

intra-particle diffusion is not the only rate-controlling step, and external mass transfer also occurs simultaneously (Liang et al. 2019; Abdel-Salam et al. 2017).

Based on the data in Table 2, it can be concluded that there are 2 steps that describe the transfer of CBB and PIs from the solution to the external surface of the adsorbent and further directed diffusion from the adsorbate to the active sites of each adsorbent through interactions with the active functional groups of the adsorbent. The adsorption mechanism can be explained in 2 different ways: diffusion through the pores of the adsorbent and electrostatic interaction with positively charged functional groups resulting from the modification of SD-Alg with CTACl to become SD-Alg-CTA (Ebadollahzadeh and Zabihi 2020; Buhani et al. 2023a). The results of the IPD kinetic model analysis are consistent with the previously discussed pseudo-second-order kinetic model.

Equilibrium adsorption isotherms

Isotherm adsorption studies, which depict the interaction between adsorbent and adsorbate at a specific temperature under equilibrium conditions, are generally necessary for designing the adsorption mechanism (Jais et al. 2021). The adsorption isotherm patterns of CBB and PIs dyes on SD-Alg, SD-Alg-Na, and SD-Alg-CTA were investigated by analyzing the data relationship between C_o (mg L^{-1}) exposed to the amount of CBB and PIs adsorbed (mmol g^{-1}) as shown in Fig. 9. The data presented in Fig. 9 were analyzed using the Langmuir (Eq. 9), Freundlich (Eq. 10), Dubinin-Raduskevich (D-R) Eq. (11), and Temkin Eq. (12) adsorption isotherm models.

$$\frac{1}{q_e} = \frac{1}{q_m K_L C_e} + \frac{1}{q_m} \quad (9)$$

$$\log q_e = \log K_F + \frac{1}{n} \log C_e \quad (10)$$

$$\ln q_e = q_{DR} - 2B_{DR} RT \ln(1 + 1/C_e) \quad (11)$$

$$q_e = \frac{RT}{b_{Te}} \ln(K_{Te} C_e) \quad (12)$$

$$\Delta G^\circ = -RT \ln K_L \quad (13)$$

where C_e (mg L^{-1}) is the equilibrium concentration of CBB or phosphate ion solution, q_e (mmol g^{-1}) is the adsorption capacity of CBB or PIs at equilibrium, q_m is the monolayer adsorption capacity of the adsorbent, and K_L is the equilibrium constant, including the affinity of binding sites (L mg^{-1}). Furthermore, K_F ($(\text{mg g}^{-1}) (\text{L mg}^{-1})^{1/n}$) is the adsorption capacity factor, and n is the intensity factor, with the

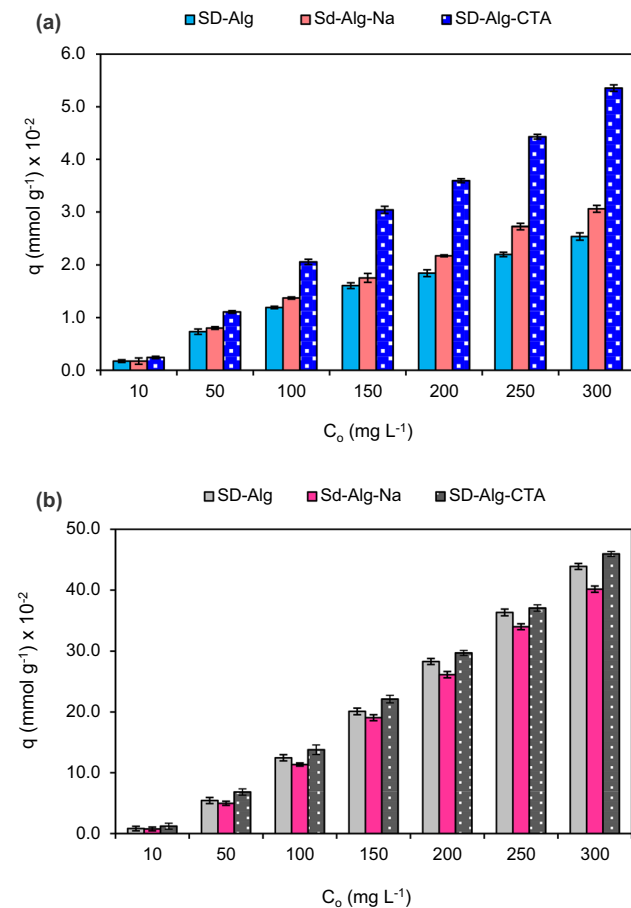


Fig. 9 Graph illustrating the relationship between C_o (mg L^{-1}) and the amount of **a** CBB and **b** PIs adsorbed (q) (mmol g^{-1}) (adsorbent mass: 0.1 g; solution volume: 25 mL; temperature: 27 ± 1 °C; agitation speed: 150 rpm; pH: CBB dye (pH 5) and PIs (pH 4); time: 120 min)



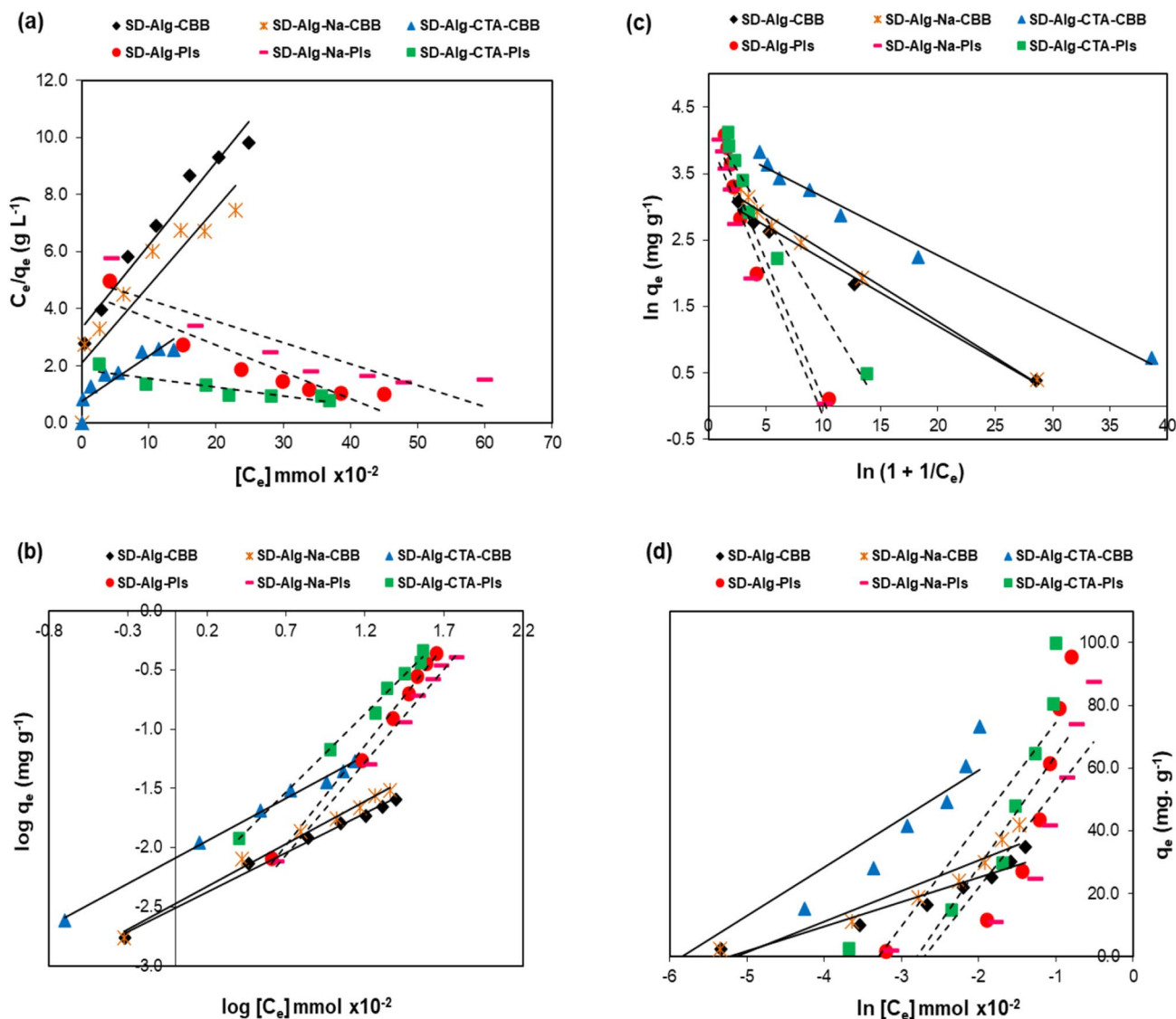


Fig.10 The linear equations of the adsorption isotherm models of the CBB and PIs on the SD-Alg, SD-Alg-Na, and SD-Alg-CTA with the adsorption isotherm model of **a** Langmuir, **b** Freundlich, **c** Dubinin-Radushkevich, and **d** Temkin

value of n ranging between 1 and 10 (Ho and McKay 2002). Furthermore, q_{DR} and B_{DR} are the D-R isotherm constants in mg g^{-1} and $\text{mol}^2 \text{kJ}^{-2}$ respectively, b_{Te} is the Temkin constant related to the heat adsorption (J mol^{-1}), K_{Te} is the equilibrium binding constant L g^{-1} , R is the gas constant ($8.314 \text{ kJ mol}^{-1}$), and T is the absolute temperature (K).

The selection of the adsorption isotherm models aims to investigate the tendency of the adsorption patterns of CBB and PIs with SD-Alg, SD-Alg-Na, and SD-Alg-CTA. The Langmuir adsorption isotherm model assumes that there is a certain number of active sites on the adsorbent surface proportional to the surface area, the adsorbent surface is uniform, and the adsorption process is monolayer

(Xin et al. 2012; Larraza et al. 2012). The Freundlich isotherm model is an empirical equation employed for heterogeneous systems and adsorption at multilayers (Shao et al. 2016). Therefore, the results of the data analysis using both adsorption isotherm models can indicate the tendency of the adsorption process to occur physically or chemically. The D-R (Dubinin-Radushkevich) isotherm model can be used to explain adsorption occurring on both homogeneous and heterogeneous surfaces. This model assumes that adsorption takes place on a homogeneous adsorption layer. Meanwhile, the Temkin isotherm model explains that the heat of adsorption decreases linearly with



Table 3 Energy and adsorption isotherm parameters of CBB dye and PIs on SD-Alg, SD-Alg-Na, SD-Alg-CTA (mmol g⁻¹) (adsorbent mass: 0.1 g; solution volume: 25 mL; temperature: 27 ± 1 °C; agitation speed: 150 rpm; pH: CBB dye (pH 5) and PIs (pH 4); time: 120 min)

Adsorbate	CBB			PIs		
	SD-Alg	SD-Alg-Na	SD-Alg-CTA	SD-Alg	SD-Alg-Na	SD-Alg-CTA
Parameters						
ΔG_{ads}^0 (kJ mol ⁻¹)	-54.268	-63.545	-75.840	-75.310	-67.240	-69.675
q_{exp} (mmol g ⁻¹) × 10 ⁻²	2.541	3.061	5.353	43.887	40.150	45.938
Adsorption isotherm models						
Langmuir						
q_m (mmol g ⁻¹) × 10 ⁻²	3.435	3.687	6.274	10.560	13.333	32.468
K_L (L mmol ⁻¹) × 10 ⁻¹	8.801	12.778	20.919	1.048	1.482	1.634
R^2	0.956	0.828	0.822	0.873	0.806	0.822
Freundlich						
K_F ((mg g ⁻¹)(L mg ⁻¹) ^{1/n}) × 10 ⁻¹	30.000	33.258	81.395	6.842	6.989	34.689
n	1.504	1.381	1.393	0.593	0.638	0.755
R^2	0.995	0.989	0.995	0.992	0.993	0.994
Dubinin-Raduskevich						
q_{DR} (mg g ⁻¹)	26.722	30.554	55.919	74.448	58.657	72.894
B_{DR} × 10 ⁻⁶	1.990	1.805	1.474	7.062	7.074	4.837
R^2	0.976	0.989	0.985	0.9340	0.938	0.957
Temkin						
b_{Te} (J mol ⁻¹)	3.135	3.919	6.211	14.313	12.497	13.029
a_{Te} (L g ⁻¹)	1.053	1.082	1.252	1.773	1.525	1.749
R^2	0.917	0.897	0.865	0.717	0.748	0.768

increasing interaction between the adsorbate and adsorbent (Buhani et al. 2019). The results of the data analysis with the adsorption isotherm models and adsorption parameters for CBB and PIs are presented in Fig. 10 and Table 3.

The adsorption parameters for CBB and PIs on SD-Alg, SD-Alg-Na, and SD-Alg-CTA in Fig. 10 and Table 3 indicate that the coefficient of regression (R^2) for the Freundlich adsorption isotherm model tends to be larger than that for the Langmuir, D-R, and Temkin isotherm. This suggests that the adsorption isotherms of CBB and PIs are more suitable for the Freundlich adsorption isotherm model. The Freundlich adsorption isotherm describes that the adsorption process of the adsorbate occurs on a heterogeneous surface with a multilayer structure. This indicates that the adsorption of CBB and PIs dyes on SD-Alg, SD-Alg-Na, and SD-Alg-CTA is more dominated by physical interactions through cation exchange or weak chemical interactions via electrostatic interactions in an aqueous medium. In other words, it can be stated that adsorption occurs through several stages. This aligns with the pseudo-second-order kinetic model, which assumes that chemisorption occurs in multiple stages through electron exchange between the adsorbate and adsorbent via electrostatic interactions (Aqdam et al. 2021; Buhani et al.

Table 4 Bi-component adsorption parameters of CBB and PIs dyes on SD-Alg, SD-Alg-Na, SD-Alg-CTA (adsorbent mass: 0.1 g; solution volume: 25 mL; C_0 (CBB + PIs) = 0.0–0.35 mmol L⁻¹; temperature: 27 ± 1 °C; agitation speed: 150 rpm; pH: 5; time: 120 min)

Adsorbent	q_m (mmol. g ⁻¹) × 10 ⁻²	bj (L.mmol ⁻¹) × 10 ⁻⁴	
		b_1 (CBB)	b_2 (PIs)
SD-Alg	6.803	1.900	11.000
SD-Alg-Na	52.632	1.700	40.900
SD-Alg-CTA	90.909	2.300	57.100

2021b). The adsorption of CBB and PIs dyes by the 3 adsorbents does not occur solely through chemical or physical interactions but is a combination of both (Buhani et al. 2019; Dhawane et al. 2017). This is also supported by the magnitude of the ΔG_{ads}^0 values (Eq. 13) obtained from the interaction between the adsorbent and adsorbate as listed in Table 3, with respective ranges for CBB between -54 and -76.00 kJ mol⁻¹ and for PIs between -67 and -75 kJ mol⁻¹. From this free energy data, it can be inferred that the modification of SD-Alg with CTA⁺ ions causes the interaction between adsorbent and adsorbate to become increasingly exothermic.



Furthermore, the data in Table 3 show adsorption parameters such as the adsorption capacity (q_m), KL , and KF values for each adsorbate on the adsorbent, indicating that SD-Alg-CTA has higher values compared to SD-Alg and SD-Alg-Na. This indicates that anionic CBB and PIs are more suitable for the SD-Alg-CTA adsorbent, which has a positive surface charge. The interactions between CBB and PIs with SD-Alg-CTA are dominated by electrostatic interactions (Buhani et al. 2023b). In this case, the adsorption mechanism can be explained in 2 different ways: diffusion through the pores of the adsorbent and electrostatic interactions with positively charged functional groups resulting from the modification of SD-Alg with the surfactant CTACl, producing SD-Alg-CTA rich in positive charge.

Bi-component adsorption

The competition of CBB and PIs adsorption onto SD-Alg-CTA was studied by conducting adsorption on a bi-component mixture of CBB and PIs, which was analyzed using the Langmuir isotherm equation model for a binary mixture (Eq. 14) (Fagundes-Klen et al. 2007; Kleinubing et al. 2011).

$$q_1^* = \frac{q_m C_1^* b_1}{1 + b_1 C_1^* + b_2 C_2^*} \quad (14)$$

where b_1 (CBB) and b_2 (PIs) are the binary Langmuir isotherm constants (Olusegun et al. 2020). The results of the adsorption data on the bi-component mixture (CBB and PIs)

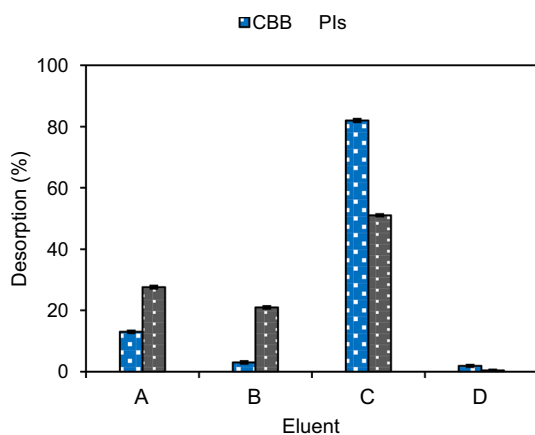


Fig. 11 Graph depicting the relationship between eluent types and the % desorption of CBB and PIs from SD-Alg-CTA using eluents H₂O **A**, 0.1 M KNO₃ **B**, 0.1 M HCl **C**, and 0.1 M Na₂EDTA **D** under adsorption conditions: adsorbent mass: 0.1 g; solution volume: 25 mL; temperature: 27 ± 1 °C; agitation speed: 150 rpm; pH: CBB dye (pH 5) and PIs (pH 4); time: 120 min

by SD-Alg-CTA using the Langmuir isotherm equation for a binary mixture are presented in Table 4.

In Table 4, it can be observed that the q_m values for bi-component adsorption on the 3 adsorbents, SD-Alg, SD-Alg-Na, and SD-Alg-CTA, are 6.803×10^{-2} , 52.632×10^{-2} , and 90.909×10^{-2} mmol·g⁻¹, respectively. This aligns with the q_m values obtained for mono-component adsorption (Table 3). In mono-component adsorption, there is no competition for adsorption, whereas in bi-component adsorption, it is assumed that there is competition for adsorption between CBB and PIs in occupying the active sites of the adsorbent, whether in the form of pores or active groups (Buhani et al. 2021b). Furthermore, in Table 4, it is observed that all 3 adsorbents produce values where $b_{1(\text{CBB})} < b_{2(\text{PIs})}$. This indicates that PIs are more dominantly adsorbed compared to the CBB dye on SD-Alg-CTA in bi-component adsorption. The CBB dye (M_R C₄₇H₄₉N₃NaO₇S₂ = 855.028 g mol⁻¹) has a larger size than PIs (M_R KH₂PO₄ = 136.09), making it less mobile and slower to compete compared to PIs.

Proposed adsorption mechanism

The mechanism of the reaction occurring during the adsorption of CBB and PIs dyes by SD-Alg-CTA was studied by performing sequential desorption using several eluents based on their ability to elute the adsorbed adsorbate in the adsorbent (Buhani et al. 2023a, b, c). In this study, the adsorbed CBB or PIs dyes were eluted with H₂O (A), 0.1 M KNO₃ (B), 0.1 M HCl (C), and 0.1 M Na₂EDTA (D) (Fig. 11), with their strengths increasing sequentially to release the physically adsorbed CBB or PIs dyes, ion exchange, electrostatic interactions, and complexes.

In Fig. 11, it can be observed that the CBB dye adsorbed by SD-Alg-CTA can be released by eluents in the following order: 0.1 M HCl (82.023%) > H₂O (13.057%) > KNO₃

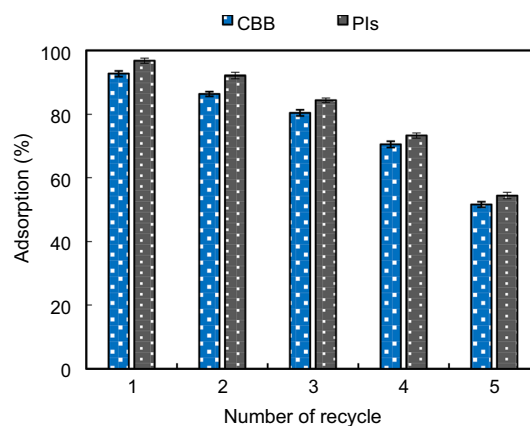


Fig. 12 Reutilization of SD-Alg-CTA in 5 adsorption–desorption cycles for CBB and PIs



Table 5 Comparison of the adsorption capacities of several adsorbents for CBB and PIs

Adsorbent	CBB (mg g ⁻¹)	Refs.	Adsorbent	PIs (mg g ⁻¹)	Refs.
Wheat brand	6.40	(Ata et al. 2012)	LDH-biochars	21.8	(Huang et al. 2023)
CuO/C nanocomposites	9.09	(Bhavyasree and Xavier. 2021)	Fe ₃ O ₄ @SiO ₂ -La	27.8	(Lai et al. 2016)
α-Chitin nanoparticles	8.55	(Dhananasekaran et al. 2016)	Biomass gasification	30.2	(Kilpimaa et al. 2015)
Activated carbon (<i>Nigella sativa</i> L)	14.49	(Abdel-Ghani et al. 2017)	Titania/GO	33.11	(Sakulpaisan et al. 2016)
Coir pith	31.80	(Prasad et al. 2008)	Activated biochar	37.00	(Isiuku et al. 2021)
Nanohydrogel	31.20	(Sharma et al. 2017)	Al-modified biochar	57.49	(Yin et al. 2018)
Unactivated carbon modified	68.317	(Buhani et al. 2023c)	Amine cross-linked tea waste	98.72	(Qiao et al. 2019)
SD-Alg-CTA	45.773	This work	SD-Alg-CTA	62.476	This work

(3.030%) > 0.1 M Na₂EDTA (1.890%). The same trend is observed for the desorption of PIs, with the order of eluents and % desorption as follows: 0.1 M HCl (51.090%) > H₂O (27.560%) > KNO₃ (20.933%) > 0.1 M Na₂EDTA (0.417%). From this data, it can be inferred that the interaction of CBB and PIs dyes with SD-Alg-CTA follows a similar trend, dominated by electrostatic interactions and followed by physical interactions (trapping mechanism). This is consistent with the results of pseudo-second-order adsorption kinetics and Freundlich adsorption isotherm models. Furthermore, 3 main processes occur during the adsorption of an adsorbate by an adsorbent: physical adsorption, precipitation, complexation, and pore filling (Fagbohunge et al. 2017).

The mechanism of adsorption of an adsorbate by an adsorbent in a solution is influenced by several factors such as the surface charge of the adsorbent, the nature and type of interactions between the active groups of the adsorbent and the adsorbate, such as electrostatic attraction, hydrogen bonding, ion exchange, acid–base interactions, as well as covalent bonds and complexes (Zhang et al. 2019). The electrostatic interaction mechanism becomes key in the adsorption process of ionizable organic compounds onto the adsorbent surface, indicating a positive charge through electrostatic interactions. However, the success of this mechanism in attracting or repelling organic pollutants is highly influenced by the ionic strength and pH value of the solution. These factors play a crucial role because they enhance the electrostatic interaction of repulsion between the adsorbate and adsorbent when they both have similar charges (Ambaye et al. 2021). In this case, the surface of SD-Alg-CTA contains positively charged active sites from HDTMA⁺ ions, thus dominantly interacting strongly with negatively charged CBB or PIs through electrostatic interactions, in addition to other physical and chemical interactions.

Regeneration of SD-Alg-CTA adsorbent

The technology of cost-effective and environmentally friendly adsorbent modification is highly essential, including the development of adsorbents that can be regenerated or reused in multiple adsorption cycles. The ability of an adsorbent to be used repeatedly is a crucial aspect in wastewater treatment, as it significantly contributes to cost savings in treating water containing pollutants. To assess the regenerative capacity of SD-Alg-CTA as an adsorbent, adsorption–desorption cycles were conducted for five repetitions, as shown in Fig. 12. In this study, the release of CBB and PIs dyes from SD-Alg-CTA using a 0.1 M HCl solution as the eluent was quite effective, involving proton substitution for CBB and PIs dyes as cations (Varghese et al. 2017; Buhani et al. 2023b).

From Fig. 12, it can be observed that in the third repetition of adsorption–desorption cycles, the SD-Alg-CTA still retains respective adsorption capacities of 80% for CBB and 84% for PIs. The regeneration capacity of SD-Alg-CTA decreases over several cycles (approximately 10% reduction in the fourth cycle), and in the fifth cycle, it reaches 52% for CBB and 54% for PIs. This is attributed to the incomplete release of adsorbate still attached to the adsorbent, and it is assumed that damage occurs on the adsorbent surface due to interaction with the eluent and neutralization processes. The assessment of the lifespan through adsorption–desorption equilibrium data confirms the feasibility of reusing SD-Alg-CTA as an effective and recyclable adsorbent. The reusability of this adsorbent is advantageous for continuous industrial applications that require repeated use of the adsorbent.

Comparison of adsorption capacity with other adsorbents

Table 5 shows the comparison of adsorption capacities of SD-Alg-CTA for CBB and PIs with previously documented

adsorbents. The information in the table depicts that SD-Alg-CTA exhibits high effectiveness as an adsorbent for both CBB and PIs, especially when compared to other adsorbents listed in Table 5. The comparison of adsorption performance of SD-Alg-CTA clearly demonstrates the synergistic effect of the precursor. Addition of cationic surfactant CTACI into algal biomass enables enhanced adsorption towards anions such as CBB and PIs. Modification of SD-Alg with cationic surfactant shows a significant improvement in its ability to attract anionic dye molecules like CBB and PIs. This is due to the formation of positive charges on the surface of SD-Alg-CTA, which enhances the adsorption of CBB and PIs through electrostatic interactions.

Conclusion

In this study, the modification of the macro-alga *Sargassum duplicatum* with the cationic surfactant CTACI has been successfully achieved. The modification procedure is straightforward and takes place at room temperature, resulting in an adsorbent that is highly effective in adsorption CBB and PIs in both mono-component and bi-component forms. The optimum adsorption conditions occur at pH 5 for CBB dye and at pH 4 for PIs, with respective contact times of 120 and 150 min. The adsorption of CBB and PIs by SD-Alg-CTA tends to follow the pseudo-second-order kinetic model and Freundlich isotherm adsorption model. The adsorption capacities (q_m) for the mono-component adsorption of CBB and PIs by SD-Alg-CTA are 6.27×10^{-2} and 32.468×10^{-2} mmol g⁻¹, respectively, while the q_m for the bi-component mixture is 90.909 mmol g⁻¹. SD-Alg-CTA adsorbent can be reused in 3 cycles of adsorption–desorption with adsorption efficiencies for CBB and PIs exceeding 80%. The SD-Alg-CTA material has significant potential for development due to its effective adsorption, easy manufacturing procedure, and reusability. This provides an advantage in industrial applications that require repeated use of the adsorbent.

Acknowledgements This research was supported and funded by The Higher Education for Technology and Innovation (HETI) Project Universitas Lampung for funding this study based on Research innovation and collaboration program 2023-2024 (Contract numbers: 10606/UN26/KS.00.00/2023).

Authors contribution Buhani: conceptualization, methodology, investigation, data curation, writing original draft, review and editing. Suharso: conceptualization, methodology, investigation, data curation, and writing original draft. Ahmad Barep Prayogo: methodology, investigation, data curation, and data analysis. Sumadi: methodology, investigation, and data curation. Sutarto: methodology, investigation, and data curation.

Data availability The data supporting the findings of this study are reported within the article.

Declarations

Conflict of interest The authors declare no competing interests.

References

- Abd El-Ghaffar MA, Abdel-Wahab ZH, Elwakeel KZ (2009) Extraction and separation studies of silver(I) and copper(II) from their aqueous solution using chemically modified melamine resins. *Hydrometallurgy* 9:27–34. <https://doi.org/10.1016/j.hydromet.2008.07.008>
- Abdel-Ghani NT, El-Chaghaby GA, Rawash ESA, Lima EC (2017) Adsorption of Coomassie Brilliant Blue R-250 dye onto novel activated carbon prepared from *Nigella sativa* L. waste: Equilibrium, kinetics and thermodynamics running title: Adsorption of Brilliant Blue dye onto *Nigella sativa* L. waste activated carbon. *J Chil Chem Soc* 62:3505–3511. <https://doi.org/10.4067/S0717-97072017000200016>
- AbdEl-Salam AH, Ewais HA, Basaleh AS (2017) Silver nanoparticles immobilized on the activated carbon as efficient adsorbent for removal of crystal violet dye from aqueous solutions, A kinetic study. *J Mol Liq* 248:833–841. <https://doi.org/10.1016/j.molliq.2017.10.109>
- Adegoke KA, Akinnawo SO, Adebunsi TA, Ajala OA, Adegoke RO, Maxakato NW, Bello OS (2023) Modified biomass adsorbents for removal of organic pollutants: a review of batch and optimization studies. *Int J Environ Sci Technol* 20:11615–11644. <https://doi.org/10.1007/s13762-023-04872-2>
- Aharoni C, Tompkins F (1970) Kinetics of adsorption and desorption and the Elovich equation. In: C Aharoni, FC Tompkins (eds) *Advances in catalysis*, Elsevier, 21:1–49 [https://doi.org/10.1016/S0360-0564\(08\)60563-5](https://doi.org/10.1016/S0360-0564(08)60563-5)
- Ahmad MA, Ahmed NB, Adegoke KA, Bello OS (2019) Sorption studies of methyl red dye removal using lemon grass (*Cymbopogon citratus*). *Chem Data Collect* 22:100249. <https://doi.org/10.1016/j.cdc.2019.100249>
- Ai L, Zhang C, Liao F, Wang Y, Li M, Meng L, Jiang J (2011) Removal of methylene blue from aqueous solution with magnetite loaded multi-wall carbon nanotube: Kinetic, isotherm and mechanism analysis. *J Hazard Mater* 198:282–290. <https://doi.org/10.1016/j.jhazmat.2011.10.041>
- Al-Odayni AB, Alsubaie FS, Abdu NAY, Al-Kahtani HM, Saeed WS (2023) Adsorption kinetics of methyl orange from model polluted water onto n-doped activated carbons prepared from n-containing polymers. *Polymers* 15:1983. <https://doi.org/10.3390/polym15091983>
- Altikatoglu M (2011) Enhanced stability and decolorization of coomassie brilliant blue r-250 by dextran aldehyde-modified horseradish peroxidase. *Artif Cell Blood Sub* 39:185–190. <https://doi.org/10.3109/10731199.2010.533124>
- Ambaye TG, Vaccari M, van Hullebusch ED, Amrane A, Rtimi S (2021) Mechanisms and adsorption capacities of biochar for the removal of organic and inorganic pollutants from industrial wastewater. *Int J Environ Sci Technol* 18:3273–3294. <https://doi.org/10.1007/s13762-020-03060-w>
- Aqdam SR, Otzen DE, Mahmoodi NM, Morshedi D (2021) Adsorption of azo dyes by a novel bio-nanocomposite based on whey protein nanofibrils and nanoclay: Equilibrium isotherm and kinetic modelling. *J Colloid Interface Sci* 602:490–503. <https://doi.org/10.1016/j.jcis.2021.05.174>
- Ata S, DinMI M, Rasool A, Qasim I, Mohsin IU (2012) Equilibrium, thermodynamics, and kinetic sorption studies for the removal of



- coomassie brilliant blue on wheat bran as a lowcost adsorbent. *J Anal Method Chem* 1:1–8. <https://doi.org/10.1155/2012/405980>
- Bhavayaree PG, Xavier TS (2021) Adsorption studies of methylene blue, coomassie brilliant blue, and congo red dyes onto CuO/C nanocomposites synthesized via Vitex negundo Linn leaf extract. *CRGSC* 4:100161. <https://doi.org/10.1016/j.crgsc.2021.100161>
- Bingol A, Aslan A, Cakici A (2009) Biosorption of chromate anions from aqueous solution by a cationic surfactant-modified lichen (*Cladonia Raniformis* (L)). *J Hazard Mater* 161:747–752. <https://doi.org/10.1016/j.jhazmat.2008.04.018>
- Boparai HK, Joseph M, O'Carroll DM (2011) Kinetics and thermodynamics of cadmium ion removal by adsorption onto nano zerovalent iron particles. *J Hazard Mater* 186:458–465. <https://doi.org/10.1016/j.jhazmat.2010.11.029>
- Buhani S, Aditiya I, Kausar RA, Sumadi R (2019) Production of a *Spirulina* sp. algae hybrid with a silica matrix as an effective adsorbent to absorb crystal violet and methylene blue in a solution. *Sustain Environ Res* 29:1–11. <https://doi.org/10.1186/s42834-019-0027-2>
- Buhani S, Miftahza N, Permatasari D, Sumadi, (2021a) Improved adsorption capacity of *Nannochloropsis* sp. through modification with cetyltrimethylammonium bromide on the removal of methyl orange in solution. *Adsorp Sci Technol* 2021:1–14. <https://doi.org/10.1155/2021/1641074>
- Buhani WTA, Suharso S, Ansori M (2021b) Application of modified green algae *Nannochloropsis* sp. as adsorbent in the simultaneous adsorption of methylene blue and Cu (II) cations in solution. *Sustain Environ Res* 31:1–12. <https://doi.org/10.21203/rs.3.rs-64063/v2>
- Buhani DJS, Fajriyah NS, Rilyanti M, Suharso S, Elwakeel KZ (2023a) Modification of non-activated carbon from rubber fruit shells with 3-(aminopropyl)-triethoxysilane and its adsorption study on coomassie brilliant blue and methylene blue in solution. *Water Air Soil Pollut* 234:578. <https://doi.org/10.1007/s11270-023-06506-2>
- Buhani I, Suharso S, Sutarto AHM, Elwakeel KZ (2023b) Cationic surfactant-modified *Tetraselmis* sp. for the removal of organic dyes from aqueous solution. *Molecules* 28:7839. <https://doi.org/10.3390/molecules28237839>
- Buhani NPO, Suharso S, Sumadi SIS, Zulaicha AS (2023c) Modification of *Spirulina* sp. algae by exchanging Na⁺ cations and hexadecyltrimethylammonium⁺ (HDMTA)⁺ for removal of methyl orange and crystal violet dyes from solution. *J Iran Chem Soc* 20:2363–2372. <https://doi.org/10.1007/s13738-023-02844-4>
- Dhananasekaran S, Palanivel R, Pappu S (2016) Adsorption of methylene blue, bromophenol blue, and coomassie brilliant blue by α -chitin nanoparticles. *J Adv Res* 7:113–124. <https://doi.org/10.1016/j.jare.2015.03.003>
- Dhawane SH, Khan AA, Singh K, Tripathi A, Hasda R, Halder G (2017) Insight into optimization, isotherm, kinetics, and thermodynamics of fluoride adsorption onto activated alumina. *Environ Prog Sustain Energi* 37:766–776. <https://doi.org/10.1002/ep.12814>
- Dogan M, Abak H, Alkan M (2009) Adsorption of methylene blue onto hazelnut shell: kinetics, mechanism and activation parameters. *J Hazard Mater* 164:172–181. <https://doi.org/10.1016/j.jhazmat.2008.07.155>
- Dolar D, Košutić KV (2011) RO/NF Treatment of wastewater from fertilizer factory—removal of fluoride and phosphate. *Desalination* 265:237–241. <https://doi.org/10.1016/j.desal.2010.07.057>
- Ebadollahzadeh H, Zabihi M (2020) Competitive adsorption of methylene blue and Pb (II) ions on the nano-magnetic activated carbon and alumina. *Mater Chem Phys* 248:122893. <https://doi.org/10.1016/j.matchemphys.2020.122893>
- Elgarahy AM, Elwakeel KZ, Mohammad SH, Elshoubaky GA (2021) A critical review of biosorption of dyes, heavy metals and metalloids from wastewater as an efficient and green process. *Clean Eng Technol* 4:100209. <https://doi.org/10.1016/j.clet.2021.100209>
- Elwakeel KZ, Shahat A, Khan ZA, Alshitari W, Guibal E (2020) Magnetic metal oxide-organic framework material for ultrasonic-assisted sorption of titan yellow and rose Bengal from aqueous solutions. *Chem Eng J* 392:123635. <https://doi.org/10.1016/j.cej.2019.123635>
- Escalona Platero E, Peñarroya Mentrut M, Otero Areán C, Zecchina A (1996) FTIR studies on the acidity of Sulfated Zirconia prepared by thermolysis of zirconium sulfate. *J Catal* 162(2):268–276. <https://doi.org/10.1006/jcat.1996.0284>
- Fagbohunge MO, Herbert BMJ, Hurst L, Ibeto CN, Li H, Usmani SQ, Semple KT (2017) The challenges of anaerobic digestion and the role of biochar in optimizing anaerobic digestion. *Waste Manage* 61:236–249. <https://doi.org/10.1016/j.wasman.2016.11.028>
- Fagundes-Klen MR, Ferri P, Martins TD, Tavares CRG, Silva EA (2007) Equilibrium study of the binary mixture of cadmium-zinc ions biosorption by the *Sargassum filipendula* species using adsorption isotherms models and neural network. *Biochem Eng J* 34:136–146. <https://doi.org/10.1016/j.bej.2006.11.023>
- Ferreira A, Mota A, Oliveira A, Rodrigues F, Pacífico S, Da Silva J, Abagaro B, Saraiva G, De Castro A, Teixeira R (2019) Equilibrium and kinetic modelling of adsorption: evaluating the performance of an adsorbent in softening water for irrigation and animal consumption. *Rev Virtual Quim* 11:1752–1766. <https://doi.org/10.21577/1984-6835.20190123>
- Flores-Chaparro CE, Ruiz LFC, de la Torre MCA, Huerta-Diaz MA, Rangel-Mendez JR (2017) Biosorption removal of benzene and toluene by 3 dried Macroalgae at different ionic strength and temperatures: algae biochemical composition and kinetics. *J Environ Manage* 193:126–135. <https://doi.org/10.1016/j.jenvman.2017.02.005>
- Guler UA, Ersan M, Tuncel E, Düğenci F (2016) Mono and simultaneous removal of crystal violet and safranin dyes from aqueous solutions by HDTMA-modified *Spirulina* sp. *Process Saf Environ* 99:194–206. <https://doi.org/10.1016/j.psep.2015.11.006>
- Hamoudi S, Belkacemi K (2013) Adsorption of nitrate and phosphate ions from aqueous solutions using organically-functionalized silica materials: kinetic modelling. *Fuel* 110:107–113. <https://doi.org/10.1016/j.fuel.2012.09.066>
- Harris PO, Ramelow GJ (1990) Binding of metal ions by particulate biomass derived from chlorella vulgaris and scenedesmus quadricauda. *Environ Sci Technol* 24:220–228. <https://doi.org/10.1021/es00072a011>
- Ho YS, Porter JF, McKay G (2002) Equilibrium isotherm studies for the sorption of divalent metal ions onto peat: copper, nickel, and lead single component systems. *Water Air Soil Poll* 141:1–33. <https://doi.org/10.1023/A:1021304828010>
- Huang R, Liu Q, Zhang L, Yang B (2015) Utilization of cross-linked chitosan/bentonite composite in the removal of methyl orange from aqueous solution. *Water Sci Technol* 71:174–182. <https://doi.org/10.2166/wst.2014.478>
- Huang W, Zhang Y, Li D (2017) Adsorptive removal of phosphate from water using mesoporous materials: A review. *J Environ Manage* 193:470–482. <https://doi.org/10.1016/j.jenvman.2017.02.030>
- Huang W-H, Chang Y-J, Wu R-M, Chang J-S, Chuang X-Y, Lee D-J (2023) Type-wide biochars loaded with Mg/Al layered double hydroxide as adsorbent for phosphate and mixed heavy metal ions in water. *Environ Res* 224:115520. <https://doi.org/10.1016/j.envres.2023.115520>
- Hussain S, Kamran M, Khan SA, Shaheen K, Shah Z, Suo H, Khan Q, Shah AB, Rehman WU, Al-Ghamdi YO, Ghani U (2021) Adsorption, kinetics and thermodynamics studies of methyl orange dye sequestration through chitosan composites films.



- Int J Biol Macromol 168:383–394. <https://doi.org/10.1016/j.ijbiomac.2020.12.054>
- Ibrahim AO, Adegoke KA, Adegoke RO, AbdulWahab YA, Oyelami VB, Adesina MO (2021) Adsorptive removal of different pollutants using metal-organic framework adsorbents. *J Mol Liquid* 333:1–34. <https://doi.org/10.1016/j.molliq.2021.115593>
- Isiuku BO, Enyoh CE, Duru CE, Ibe FC (2021) Phosphate ions removal from aqueous phase by batch adsorption on activated (activation before carbonization) biochar derived from rubber pod husk. *CRGSC* 4:100136. <https://doi.org/10.1016/j.crgsc.2021.100136>
- Jais FM, Chee CY, Ismail Z, Ibrahim S (2021) Experimental design via NaOH activation process and statistical analysis for activated sugarcane bagasse hydrochar for removal of dye and antibiotic. *J Environ Chem Eng* 9:104829. <https://doi.org/10.1016/J.JECE.2020.104829>
- Jastrzębski W, Sitarz M, Rokita M, Bułat K (2011) Infrared spectroscopy of different phosphates structures. *Spectrochim Acta a Mol Biomol Spectrosc* 79(4):722–727. <https://doi.org/10.1016/j.saa.2010.08.044>
- Jing X, Cao Y, Zhang X, Wang D, Wu X, Xu H (2011) Biosorption of Cr(VI) from simulated wastewater using a cationic surfactant modified spent mushroom. *Desalination* 269:120–127. <https://doi.org/10.1016/j.desal.2010.10.050>
- Kilpimaa S, Runtti H, Kangas T, Lassi U, Kuokkanen T (2015) Physical activation of carbon residue from biomass gasification: novel sorbent for the removal of phosphates and nitrates from aqueous solution. *J Ind Eng Chem* 21:1354–1364. <https://doi.org/10.1016/j.jiec.2014.06.006>
- Kim S, Yun HP, Jae BL, Ho SK, Yoon E, Choi P (2020) Adsorption behavior of industrial waste biomass-based adsorbent, esterified polyethylenimine-coated polysulfone-*Escherichia coli* biomass composite fibers in aqueous solution. *J Hazard Mater* 400:123217. <https://doi.org/10.1016/j.jhazmat.2020.123217>
- Kleinubing SJ, da Silva EA, da Silva MGC, Guibal E (2011) Equilibrium of Cu(II) and Ni(II) biosorption by marine alga *Sargassum filipendula* in a dynamic system: competitiveness and selectivity. *Bioresour Technol* 102:4610–4617. <https://doi.org/10.1016/j.biortech.2010.12.049>
- Lai L, Xie Q, Chi L, Gu W, Wu D (2016) Adsorption of phosphate from water by easily separable Fe₃O₄@SiO₂ core/shell magnetic nanoparticles functionalized with hydrous lanthanum oxide. *J Colloid Interface Sci* 465:76–82. <https://doi.org/10.1016/j.jcis.2015.11.043>
- Larraza I, López-Gonzales M, Corrales T, Marcelo G (2012) Hybrid materials: Magnetite polyethylenimine-montmorillonite, as magnetic adsorbents for Cr (VI) water treatment. *J Colloid and Interface Sci* 385:1:24–33. <https://doi.org/10.1016/j.jcis.2012.06.050>
- Lee XJ, Ong HC, Ooi J, Yu KL, Tham TC, Chen WH, Ok YS (2022) Engineered macroalgal and microalgal adsorbents: Synthesis routes and adsorptive performance on hazardous water contaminants. *J Hazard Mater* 423:126921. <https://doi.org/10.1016/j.jhazmat.2021.126921>
- Leo CP, Chai WK, Mohammad AW, Qi Y, Hoedley AFA, Chai SP (2011) Phosphorus removal using nanofiltration membranes. *Water Sci Technol* 64:199–205. <https://doi.org/10.2166/wst.2011.598>
- Li Z, Jiang WT, Hong H (2008) An FTIR investigation of hexadecyl trimethylammonium intercalation into rectorite. *Spectrochim* 71:1525–1534. <https://doi.org/10.1016/j.saa.2008.05.015>
- Liang YD, He YJ, Wang TT, Lei LH (2019) Adsorptive removal of gentian violet from aqueous solution using CoFe₂O₄/activated carbon magnetic composite. *J Water Process Eng* 7:77–88. <https://doi.org/10.1016/j.jwpe.2018.11.013>
- Milledge JJ, Maneein S, López EA, Bartlett D (2020) Sargassum inundations in turks and caicos: methane potential and proximate, ultimate, lipid, amino acid, metal and metalloid analyses. *Energies* 13:1523. <https://doi.org/10.3390/en13061523>
- Nodeh HR, Sereshti H, Afsharian EZ, Nouri N (2017) Enhanced removal of phosphate and nitrate ions from aqueous media using nanosized lanthanum hydrous doped on magnetic graphene nanocomposite. *J Environ Manage* 197:265–274. <https://doi.org/10.1016/j.jenvman.2017.04.004>
- Olusegun SJ, Mohallem NDS (2020) Comparative adsorption mechanism of doxycycline and congo red using synthesized kaolinite supported CoFe₂O₄ nanoparticles. *Environ Pollut* 260:114019. <https://doi.org/10.1016/j.envpol.2020.114019>
- Onyango MS, Kuchar D, Kubota M, Matsuda H (2007) Adsorptive removal of phosphate ions from aqueous solution using synthetic zeolite. *Ind Eng Chem Res* 46:894–900. <https://doi.org/10.1021/IE060742M>
- Ozdemir S, Cirik K, Akman D, Sahinkaya E, Cinar O (2013) Treatment of azo dye-containing synthetic textile dye effluent using sulfidogenic anaerobic baffled reactor. *Bioresour Technol* 146:135–143. <https://doi.org/10.1016/j.biortech.2013.07.066>
- Prasad NR, Viswanathan S, Devi JR, Rajkumar J, Parthasarathy N (2008) Kinetics and equilibrium studies on biosorption of CBB by coir pith. *J Sci Res* 3:123–127. <http://citeseerx.ist.psu.edu/viewdoc/download?doi=10.1.1.495.7038&rep=rep1&type=pdf>
- Qiao H, Mei L, Chen G, Liu H, Peng C, Ke F, Hou R, Wan X, Cai H (2019) Adsorption of nitrate and phosphate from aqueous solution using amine cross-linked tea wastes. *Appl Surf Sci* 483:114–122. <https://doi.org/10.1016/j.apsusc.2019.03.147>
- Sakulpaisan S, Vongsetskul T, Reamouppaturm S, Luangkachao J, Tantirungrotechai J, Tangboriboonrat P (2016) Titania-functionalized graphene oxide for an efficient adsorptive removal of phosphate ions. *J Environ Manage* 167:99–104. <https://doi.org/10.1016/j.jenvman.2015.11.028>
- Saldarriaga-Hernandez S, Hernandez-Vargas G, Iqbal HMN, Barcelo D, ParraSaldivar R (2020) Bioremediation potential of Sargassum sp. biomass to tackle pollution in coastal ecosystems: circular economy approach. *Sci Total Environ* 715:136978
- Sarwa P, Verma SK (2013) Decolouration of orange G dye by microalgae *Acutodesmus obliquus* Strain PSV2 isolated from textile industrial site. *Int J Appl Sci Biotechnol* 1:247–252. <https://doi.org/10.3126/ijasbt.v1i4.9141>
- Sayadi MH, Salmani N, Heidari A, Rezaei MR (2018) Bio-synthesis of palladium nanoparticle using *Spirulina platensis* alga extract and its application as adsorbent. *Surf Interfaces* 10:136–143. <https://doi.org/10.1016/j.surfin.2018.01.002>
- Shao Y, Zhou L, Bao C, Ma J, Liu M, Wang F (2016) Magnetic responsive metal organic frameworks nanosphere with core-shell structure for highly efficient removal of methylene blue. *Chem Eng J* 283:1127–1136. <https://doi.org/10.1016/j.cej.2015.08.051>
- Sharma G, Naushad M, Kumar A, Rana S, Sharma S, Bhatnagar A, Stadler FJ, Ghfar AA, Khan MR (2017) Efficient removal of coomassie brilliant blue R-250 dye using starch/poly(alginate-chitosan) nanohydrogel. *Process Saf Environ Prot* 109:301–310. <https://doi.org/10.1016/j.psep.2017.04.011>
- Varghese SP, Babu AT, Babu B, Antony R (2017) γ -MnOOH nanorods: efficient adsorbent for removal of methylene blue from aqueous solutions. *J Water Process Eng* 19:1–7. <https://doi.org/10.1016/j.jwpe.2017.06.001>
- Xin X, Wei Q, Yang J, Yan L, Feng R, Chen G, Dua B, Li H (2012) Highly efficient removal of heavy metal ions by amine-functionalized mesoporous Fe₃O₄ nanoparticles. *J Chem Eng* 84:132–140. <https://doi.org/10.1016/j.cej.2012.01.016>
- Xu X, Gao BY, Yue QY, Zhong QQ (2010) Preparation of agricultural by-product based anion exchanger and its utilization for nitrate and phosphate removal. *Bioresour Technol* 101:8558–8564. <https://doi.org/10.1016/j.biortech.2010.06.060>



- Yadav D, Kapur M, Kumar P, Mondal MK (2015) Adsorptive removal of phosphate from aqueous solution using rice husk and fruit juice residue. *Process Saf Environ Prot* 94:402–409. <https://doi.org/10.1016/j.psep.2014.09.005>
- Yang S, Zhao Y, Ding D, Wang Y, Feng C, Lei Z, Yang Y, Zhang Z (2013) An electrochemically modified novel tablet porous material developed as adsorbent for phosphate removal from aqueous solution. *Chem Eng J* 220:367–374. <https://doi.org/10.1016/j.cej.2013.01.067>
- Yin Q, Ren H, Wang R, Zhao Z (2018) Evaluation of nitrate and phosphate adsorption on Al-modified biochar: Influence of Al content. *Sci Total Environ* 631–632:895–903. <https://doi.org/10.1016/j.scitotenv.2018.03.091>
- Yusof AM, Malek NA (2009) Removal of Cr(VI) and As(V) from aqueous solution by HDTMA modified zeolite Y. *J Hazard Mater* 162:1019–1024. <https://doi.org/10.1016/j.jhazmat.2008.05.134>
- Zhan Y, Lin J, Zhu Z (2011) Removal of nitrate from aqueous solution using cetylpyridinium bromide (CPB) modified zeolite as adsorbent. *J Hazard Mater* 186(2–3):1972–1978. <https://doi.org/10.1016/j.jhazmat.2010.12.090>
- Zhang YY, Liu Q, Yang C, Wu SC, Cheng JH (2019) Magnetic aluminum-based metal organic framework as a novel magnetic adsorbent for the effective removal of minocycline from aqueous solutions. *Environ Pollut* 255:113226. <https://doi.org/10.1016/j.envpol.2019.113226>

Springer Nature or its licensor (e.g. a society or other partner) holds exclusive rights to this article under a publishing agreement with the author(s) or other rightsholder(s); author self-archiving of the accepted manuscript version of this article is solely governed by the terms of such publishing agreement and applicable law.

